Remote sensing of crystal shapes in ice clouds

Bastiaan van Diedenhoven[1,2]

[1]Columbia University, Center for Climate System Research, 2880 Broadway, New York, NY 10025
[2]NASA Goddard Institute for Space Studies, 2880 Broadway, New York, NY 10025

Correspondence to: Bastiaan van Diedenhoven (bastiaan.vandiedenhoven@nasa.gov)

Abstract.

Ice crystals in clouds exist in a virtually limitless variation of geometries. The most basic shapes of ice crystals are columnar or plate-like hexagonal prisms with aspect ratios determined by relative humidity and temperature. However, crystals in ice clouds generally display more complex structures owing to aggregation, riming and growth histories through varying temperature and humidity regimes. Crystal shape is relevant for cloud evolution as it affects microphysical properties such as fall speeds and aggregation efficiency. Furthermore, the scattering properties of ice crystals are affected by their general shape, as well as by microscopic features such as surface roughness, impurities and internal structure. To improve the representation of ice clouds in climate models, increased understanding of the global variation of crystal shape and how it relates to, e.g., location, cloud temperature and atmospheric state is crucial. Here, the remote sensing of ice crystal macroscale and microscale structure from airborne and space-based lidar depolarization observations and multi-directional measurements of total and polarized reflectances is reviewed. In addition, a brief overview is given of in situ and laboratory observations of ice crystal shape as well as the optical properties of ice crystals that serve as foundations for the remote sensing approaches. Lidar depolarization is generally found to increase with increasing cloud height and to vary with latitude. Although this variation is generally linked to the variation of ice crystal shape, the interpretation of the depolarization remains largely qualitative and more research is needed before quantitative conclusions about ice shape can be deduced. The angular variation of total and polarized reflectances of ice clouds has been analyzed by numerous studies in order to infer information about ice crystal shapes from them. From these studies it is apparent that pristine crystals with smooth surfaces are generally inconsistent with the data and thus crystal impurity, distortion or surface roughness is prevalent. However, conclusions about the dominating ice shapes are often inconclusive and contradictory and are highly dependent on the limited selection of shapes included in the investigations. Since ice crystal optical properties are mostly determined by the aspect ratios of the crystal components and their microscale structure, it is advised that remote sensing applications focus on the variation of these ice shape characteristics, rather than on the macroscale shape or habit. Recent studies use databases with nearly continuous ranges of crystal component aspect ratio and/or roughness levels to infer the variation of ice crystal shape from satellite and airborne remote sensing measurements. Here, the rationale and results of varying strategies for the remote sensing of ice crystal shape are reviewed. Observed systematic variations of ice crystal geometry with location, cloud height and atmospheric state suggested by the data are discussed. Finally, a prospective is given on the future of the remote sensing of ice cloud particle shapes.

1 Introduction

Archaeological findings reveal a deeply rooted human obsession for atmospheric optical phenomena such as rainbows and ice cloud halos. Our pre-historic ancestors likely attached divine or meteorological meanings to such optical phenomena as suggested by ancient rock drawings (Ping-Yü and Needham, 1959; Sassen, 1991, 1994). Detailed observations of rainbows and ice cloud halos were later described by Aristotle and other scholars of antiquity. It took until the age of enlightenment, however, for the first qualitatively correct interpretations of these phenomena to be documented (Nussenzveig, 1977; Greenler, 1990; Tape, 1994; Tape and Moilanen, 2006). For example, it was the French physicist and priest Edme Marriotte who, in 1691, was probably the first to correctly attribute the commonly observed halo at an angle of 22° around the sun to randomly oriented hexagonal ice crystals, although his ideas did not gain much attention until being revived 116 years later by Thomas Young (Tape and Moilanen, 2006). It was later realized that this hexagonal ice model also offers explanations of parhelia ('sundogs') and other arcs, when crystals are assumed to be oriented. One can thus argue that Mariotte's interpretation of the halo observations was the first successful remote sensing of ice crystal shape.

While liquid drops generally take shape of virtually perfect spheres, the observed variety of cloud ice crystal shape is seemingly limitless (Baran, 2009). Under most atmospheric conditions and undisturbed, water ice grows as hexagonal prisms owing to its fundamental hexagonal molecular structure (generally denoted as I_h), where the growth rate of the basal and prismatic planes of the prisms are determined by temperature and humidity (Pauling, 1935; Bailey et al., 2012; Harrington et al., 2013). However, because of varying atmospheric conditions throughout crystal evolution, aggregation, fracturing, riming, and other stochastic effects, observed cloud ice crystals are generally far more complex than simple hexagonal prisms (e.g., Baran, 2009; Bailey and Hallett, 2009; Bailey et al., 2012). Moreover, recent advances in electron microscope technology allows imaging of the microstructure of ice surfaces, which reveals that roughness structures are generally prevalent (Pfalzgraff et al., 2010; Neshyba et al., 2013; Magee et al., 2014). Mixing of the hexagonal ice molecular structure with the cubical structure (denoted as I_c) can lead to such microscale roughness structures on the surfaces, in addition to more macroscale deviation of ice crystals from their fundamental hexagonal form (Kuhs et al., 2012; Malkin et al., 2012, 2015; Murray et al., 2015; Hudait and Molinero, 2016). Furthermore, sublimation and riming changes the surfaces of ice crystals (Ono, 1969; Ávila et al., 2009; Pfalzgraff et al., 2010; Magee et al., 2014).

The shape and size of cloud particles greatly affects their radiative and microphysical properties (Yang et al., 2015; Furtado et al., 2015; Fridlind et al., 2016; Baran et al., 2016; Liou and Yang, 2016). The omnipresence of clouds on Earth means that seemingly small changes in cloud particle properties can have profound effects on the radiation balance and precipitation (Stephens et al., 1990). In turn, cloud radiative properties affect the evolution of clouds owing to interactions between radiation and cloud microphysics (e.g., Gu and Liou, 2000; Gu et al., 2011; Russotto et al., 2016; Baran et al., 2016). While the dependences of radiative and microphysical properties on particle size are fairly well understood, knowledge on how they are affected by the shape of ice crystals is still limited. The current incomplete knowledge on the natural variation of ice crystal shape contributes to our inability to reliably represent ice clouds in global circulation models (GCMs). Biases in ice optical properties can lead to direct biases in modeled ice cloud radiative effects (Yi et al., 2013; van Diedenhoven et al., 2014a; Liou and Yang, 2016).

Furthermore, the relatively large uncertainties of cloud physics and the large influence of clouds on the radiation balance means that weakly constrained variables in GCM cloud physics parameterizations are generally adjusted to bring the simulated global long- and shortwave radiation in agreement with measurements (e.g., Schmidt et al., 2014). Through this process, any biases in ice particle optical properties would thus be falsely compensated by inadvertently introducing biases in cloud physical parameters. Moreover, biases in cloud particle shape and related microphysical quantities such as fall speeds can lead to biases in modeled cloud properties such as thermodynamic phase, precipitation and cloud fraction (Furtado et al., 2015). A new paradigm in ice microphysical modeling is emerging in which ice crystal shape characteristics are explicitly predicted (Hashino et al., 2007, 2011; Harrington et al., 2013), although a lack of observations for evaluation leave these models largely unconstrained. In addition to ice crystal shape, global constrains on the ice crystal size are also crucial in order to evaluate and improve the representation of clouds in models. However, the large uncertainty on the variation of ice particle shape, and thus optical properties, in turn lead to substantial uncertainties in ice particle size retrieved using satellite-based shortwave infrared measurements, such as by the Moderate Resolution Imaging Spectroradiometer (MODIS) (van Diedenhoven et al., 2014b; Holz et al., 2016). In situ and laboratory measurements of the past decades have lead to an increasingly detailed picture of the macro- and microscale structure of ice under varying conditions and nucleation processes (Bailey and Hallett, 2009). However, this picture is incomplete and likely biased, given the many technical and practical limitations of in situ and laboratory measurements and the uncertain and complex variation of ice nucleation and growth conditions and processes occurring in Earth's ice-containing clouds (cf. Bailey et al., 2012). Remote sensing observations of ice shape on global and regional scales are crucial for the evaluation and refinement of parameterizations of ice crystal nucleation and evolution derived from in situ and laboratory observations and theory.

This chapter offers a review of the current state of remote sensing of ice crystal macro- and microscale structure. We focus on remote sensing techniques based on passive total and polarized reflectance measurements. In addition, the potential of lidar with polarization capability to infer information about ice crystal shape is reviewed. A discussion on polarimetric radar is excluded here since current polarimetric radars are mostly sensitive to precipitation rather than cloud ice, and much of the polarimetric radar signal is related to particle orientation rather than shape (Miao et al., 2003). First, in section 2 we will briefly summarize the in situ and laboratory observations that serve as foundations of the retrieval approaches. Since by definition remote sensing necessitates the interpretation of measured electromagnetic radiation, we will review the optical properties of ice crystals in section 3. Active and passive techniques for the remote sensing of ice crystals shape are reviewed in section 4. A prospective will be given in section 5, before concluding the chapter in section 6.

2 In situ and laboratory measurements

In 1665, English natural philosopher Robert Hooke included some of the first detailed drawings of snow crystals in his book Micrographia (Hooke, 1665). The first detailed photographs were collected around the turn of the 20th century by enthusiasts such as Wilson Bentley who documented many snow crystals of various common and uncommon shapes (Bentley, 1927). The first known in situ aircraft observations of ice crystal shape were performed during the second world war by German meteorol-

ogist Ludwig Weickmann, who performed about 100 meteorological flights in an open cockpit airplane holding lacquer-coated shingles to capture and replicate ice crystals. Weickmann published results and their interpretation after the end of the war (Weickmann, 1945; aufm Kampe et al., 1951). To date, many in situ and laboratory observations of ice crystal shape have been conducted. Here, we will give a brief overview of the general and detailed shape characteristics measured in situ and in laboratories. Such observations are essential to direct and constrain remote sensing applications and to interpret their results.

2.1 General classification of ice habits

Crystal shapes are commonly classified according to the scheme of Magono and Lee (1966) that contains 80 classes of snow and ice crystals. This scheme in turn is based on previous work by Nakaya (1954), while a proposed expansion of the classification was recently offered by Kikuchi et al. (2013). The identified ice crystal shapes are commonly referred to as ice 'habits'. Nakaya (1954) and Magono and Lee (1966) also showed that the occurrence of certain habits could be linked to the meteorological conditions in which they grew and they provided diagrams of occurrence of certain ice habits as a function of temperature and humidity. Around the same time, laboratory experiments in cloud chambers were performed that successfully reproduced many of the observed transitions of habits at certain temperatures and humidities (aufm Kampe et al., 1951; Mason, 1953; Hallett and Mason, 1958; Mason et al., 1963). More recently, the most comprehensive habit diagram for atmospheric ice crystals was published by Bailey and Hallett (2009), which is shown in Fig. 1. As is apparent from Fig. 1, there are two major differentiating characteristics of ice crystals: (1) plate-like versus columnar structures and (2) single crystals versus polycrystalline particles. Plate-like crystals form when the basal planes grow faster than the prismatic facets, while the opposite relation of facet growth rates lead to columnar crystals. Polycrystals can form for various reasons, for example, when several crystal components grow relatively independently from a common core, when crystals aggregate, or when conditions vary during crystal growth. Comparing habits in different cloud types, one general observation is that compact and aggregated ice crystals with plate-like components often occur in tropical deep convection (e.g. Noel et al., 2004; Connolly et al., 2005; Um and McFarquhar, 2009; Baran, 2009), while bullet rosettes are often found in non-convective ("in situ") cirrus (e.g., Lawson et al., 2010; Fridlind et al., 2016).

The diagram produced by Bailey and Hallett (2009) (Fig. 1) is partly based on images of individual ice crystals taken in clouds by the Cloud Particle Imager (CPI) aircraft probe (Lawson et al., 2001, 2006). The highly successful CPI probe was designed in 1997 by SPEC inc. and can image and count particles in the size range of 15-2500 μm, with a nominal resolution of 2.3–μm. As discussed by Bailey and Hallett (2009), CPI images reveal many complex, polycrystalline shapes that were not represented by laboratory studies before. Automatic habit classification applied to the images generally yield a dominance of unclassified or 'irregular' crystals. Recently developed, more advanced classification schemes (e.g., Lindqvist et al., 2012) add more classes to previous CPI classification programs, but still yield an abundance of unclassified crystals. The general dominance of crystals classified as 'irregular' may be partly attributed to the issues with the automatic classification of 2D images (Stoelinga et al., 2007). Moreover, the CPI resolution is generally insufficient to classify small crystals into classes other than "small irregular" or 'quasi-spherical'. Although true quasi-spherical crystals have been observed (Järvinen et al., 2016), for most cases the term 'quasi-spherical' is arguably a misnomer, since on closer inspection these crystals generally appear

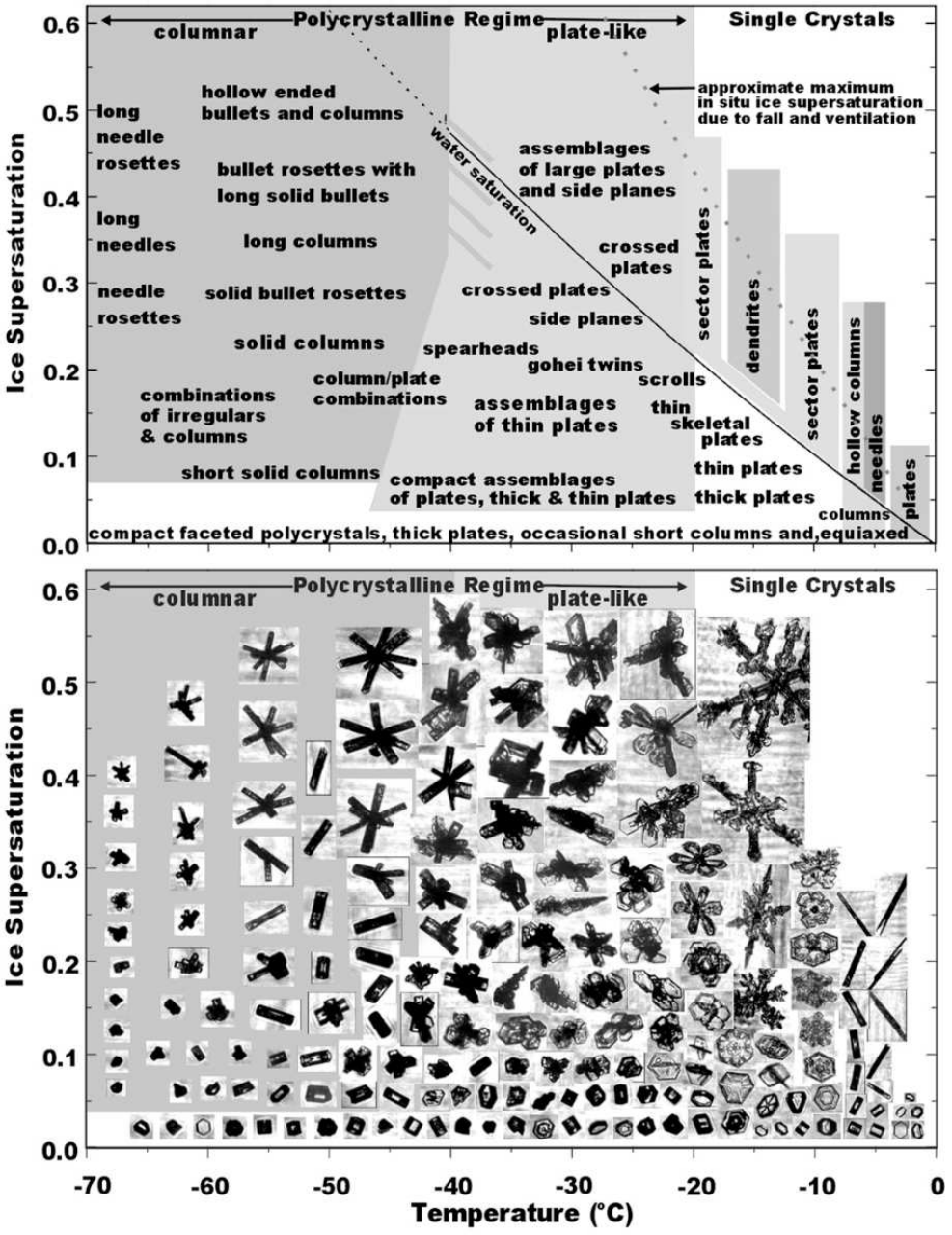

Figure 1. Diagram showing the general occurrence of ice crystal habits at varying temperatures and water vapor supersaturations with respect to ice. Habit names are in the top diagram, while example images taken by the CPI instrument are in the lower diagram. See Bailey and Hallett (2009) for more details. Figure reproduced from Bailey and Hallett (2009).

as compact polyhedra with many small facets (Gonda and Yamazaki, 1978; Bailey and Hallett, 2009) or irregular shapes with bulges and protuberances (Nousiainen et al., 2011; López and Ávila, 2012).

In summary, in situ observations are found to follow the habit diagrams as a function of temperature and humidity, but seemingly only for crystals that have grown under relatively static conditions. Given the variability of atmospheric humidity, the fact that growing ice tends to fall to warmer temperatures and the presence of up- and downdrafts in clouds, static growth conditions are an exception rather than the rule, especially in convectively-driven clouds. Furthermore, processes such as crystal aggregation, fracturing and riming add more complexity to natural crystals.

2.2 Aspect ratios of ice crystals

Traditionally, ice crystal classifications and observations have focused on the large-scale appearance of the crystals, that is, on the habits. As will be discussed in section 3, smaller scale details of the crystals are also of importance for their optical and microphysical properties, if not more important than habit. One such property is the relation between the thickness and length of particles or components of polycrystals. For a hexagonal prism, the fraction between crystal basal plane width W and prism length L is commonly referred to as aspect ratio α, which can be defined as

$$\alpha = L/W. \tag{1}$$

In this definition the aspect ratio of a column is greater than unity and that of a plate smaller than unity. However, this choice is arbitrary and confusingly some studies define aspect ratio as the inverse of Eq. 1. Alternatively, van Diedenhoven et al. (2016a) proposed a definition that limits the aspect ratio to below unity for both plates and columns, viz.

$$\alpha_{\leq 1} = \frac{\min\{L, W\}}{\max\{L, W\}}. \tag{2}$$

When this definition is used, it needs to be specified separately whether crystals are column- or plate-like. Also note that the term 'aspect ratio' is sometimes used for the ratio between two perpendicular dimensions of complex ice crystals (e.g., Korolev and Isaac, 2003) instead of the ratio between dimensions of components of those complex crystals, as the definition used here.

Several early studies on dimensional relationships of ice crystals were reported on by, e.g., Mason (1953), Ono (1969) and Auer and Veal (1970) (See Um et al. (2015) for a completer list). Auer and Veal (1970) deduced power-law relationships between the orthogonal dimensions of relatively simple particles such as plates, columns and dendrites that are still much used today as references for optical property calculations (e.g., Yang et al., 2015). Dimensions of more complex particles, such as bullet rosettes and aggregates of plates, were estimated by, e.g., Heymsfield and Andrew (1972), Mitchell and Arnott (1994), Xie et al. (2011), Um and McFarquhar (2007, 2009); Um et al. (2015) and Fridlind et al. (2016). However, most of these estimates are based on very limited data and unconstrained assumptions and different techniques can lead to conflicting results (Um et al., 2015). For plates, reported aspect ratios range from 0.01 to 0.5, while aspect ratios of columns generally range from 1.5 to 5 (Auer and Veal, 1970; Um et al., 2015). In general, aspect ratios increasingly deviate from unity as the maximum dimension increases. For bullet rosettes and their aggregates, reported aspect ratios of the arms also range from 1.5 to 5.0 and

are found to decrease towards unity with decreasing number of bullets attached to the rosettes (Um et al., 2015; Fridlind et al., 2016). Um et al. (2015) found that the aspect ratios of plates, columns and bullets in rosettes are not or only weakly sensitive to temperature, although a substantial temperature dependence may be expected from theory (Chen and Lamb, 1994; Harrington et al., 2013). Note that the crystals for which the dimensions can be determined generally comprise only a very limited subset of crystals in the observed cloud. Furthermore, the values listed above are mostly derived by the functional relationships between crystal (component) length and width that are determined from the data by the individual studies. These relationships, however, do not reflect information about the spread of data from which they are derived, which can be considerable (e.g., Um et al., 2015; Fridlind et al., 2016). For other complex crystal habits, such as aggregates of plates or columns, determining the dimensional relationships of their components from imagery is more problematic causing their aspect ratios to be more uncertain (e.g., Um and McFarquhar, 2009).

2.3 Microscale structure of ice crystals

A perfect, 'pristine', ice crystal exclusively consisting of hexagonal molecular structure (I_h) will grow smooth basal and prismatic surfaces. However, it has been long known that imperfections in the I_h mesh of growing water ice are prevalent, even under stable growth conditions (Pauling, 1935; Mason et al., 1963; Cross, 1969; Mizuno and Yukiko, 1978). Electron microscopic observations of ice crystals grown in the laboratory under different conditions reveal varying imperfections or roughness structures on the ice surfaces (Pfalzgraff et al., 2010; Sazaki et al., 2010; Neshyba et al., 2013; Magee et al., 2014). As discussed in section 3.2, such surface distortions strongly affect the scattering properties of ice crystals and need to be considered in techniques for the remote sensing of ice crystal shapes. Ice crystal surface roughness generally decreases asymmetry parameters and depresses halos in phase functions at 22° and 46° (Yang et al., 2008a; Neshyba et al., 2013; van Diedenhoven, 2014; van Diedenhoven et al., 2014a; Yang et al., 2015).

An example of roughness structures observed on laboratory-grown ice crystals under various conditions is shown in Fig. 2 (Magee et al., 2014). Magee et al. (2014) found that such roughness structures are prevalent and not confined to a narrow range of macroscopic morphology, substrate, temperature, humidity, or growth rates under most conditions. Although they did not detect a systematic dependence on the degree of supersaturation or the rate of growth, clear surface morphology differences between growing and sublimating crystals were observed. Specifically, sublimating crystals develop scalloped depressions and sharp ridges, while more linear structures were observed for growing crystals (see Fig. 2, also cf. Pfalzgraff et al., 2010). Indirect observations of roughness are provided by the Small Ice Detector-3 (SID-3) probe mounted in cloud chambers and on aircraft. This probe measures the light scattered in near-forward direction by single ice crystals. As discussed also in section 3.2, roughness structures will randomize the scattering angles at which light is scattered forward resulting in 'speckled' images measurement by the SID-3 probe, while pristine particles lead to more organized, symmetric measurements patterns. A subjective, arguably arbitrary roughness parameter is deduced from these measurements to quantify the degree of roughness. Using the SID-3 probe mounted on aircraft sampling cirrus and convective clouds, Ulanowski et al. (2014) and Schmitt et al. (2016), respectively, found that roughness is ubiquitous. Somewhat in contrast with the results of Neshyba et al. (2013) and Magee et al. (2014), cloud chamber experiments with the SID-3 measurements conducted by Schnaiter et al. (2016) indicate a

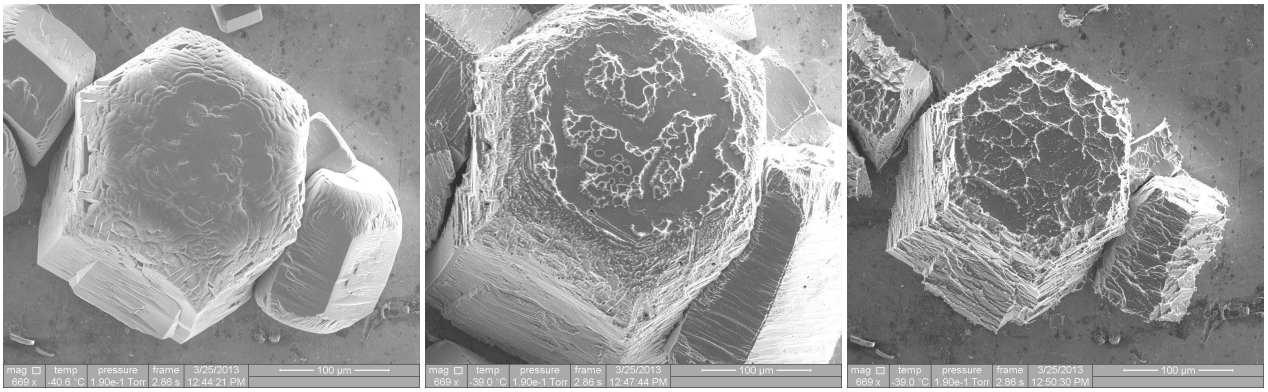

Figure 2. High-magnification images of hexagonal ice crystals acquired by environmental scanning electron microscopy revealing roughness structures on the crystal surfaces. The left image shows the crystal under vapor growth conditions. The center and right images show the crystal at the initial and a progressed stage of sublimation, respectively. For details see Magee et al. (2014). Images courtesy of Dr. Nathan Magee at The College of New Jersey.

clear correlation between the small-scale crystal complexity and the volume mixing ratio of available condensable water vapor determining the growth rate. Furthermore, Ulanowski et al. (2014) reported on similar roughness in the growth and sublimation zones of cirrus observed by the SID-3 probe, which also seems to contradict conclusions from electron microscope observations (Magee et al., 2014). Clearly, more research needs to be conducted to investigate the presence and level of roughness in the varying types of ice clouds and under varying conditions.

Although roughness structures are found to be prevalent on natural ice crystals, this appears to be in conflict with the frequent sighting of halos around the sun at 22° that are attributable to hexagonal crystals with smooth surfaces (Sassen et al., 2003; Tape and Moilanen, 2006; Verschure, 1998). For example, Sassen et al. (2003) reported that 37.3% of the daytime ice cloud observations in their ∼10 year record over Salt Lake City, Utah, showed indications of the 22° halo, with bright and prolonged halos occurring in 6% of the record. van Diedenhoven (2014) reconciled the abundance of rough ice surfaces detected with the prevelance of halos by considering cirrus clouds to contain mixtures of crystals with varying roughness levels. van Diedenhoven (2014) concluded that that the contribution by pristine crystals to the total scattering cross section needs to be greater than only about 10% in the case of compact particles or columns, and greater than about 40% for plates for the 22° halo feature to be present in scattering phase functions. These results indicate that frequent sightings of 22° halos are not inconsistent with the observed dominance of rough ice crystals. From SID-3 measurements in a halo producing cloud, Schmitt et al. (2016) also concluded that it does not require high concentrations of halo producing particles to produce an observable halo. The occurrence of 22° halo and other optical phenomena attributed to pristine crystals in some clouds but the lack there-of in other clouds illustrates that ice crystal microscale morphology is highly variable. Note that the contrast and brightness of halos also depends on the cloud optical thickness (Kokhanovsky, 2008).

Roughness structures can be effectively observed by present-day instruments, but the quantification of roughness remains elusive. One metric to quantify roughness from electron micoscope imagery was proposed by Neshyba et al. (2013) and relationships between this roughness metric and roughness parameterizations used for calculations of optical properties of rough ice crystals, as discussed in section 3.2, were also provided. Unfortunately, Magee et al. (2014) found that this metric proposed by Neshyba et al. (2013) is dependent on image magnification and resolution and is thus rather subjective. As surface roughness has profound effects on the scattering properties of ice crystals, and an increasing number of studies of the formation roughness structures under varying conditions are conducted, it is advisable that a more universal definition of roughness ought to be developed.

Apart from roughness structures on crystal surfaces, other small-scale ice crystal imperfections occur. Specifically, hollow endings in ice columns or bullets are frequently reported (Heymsfield et al., 2002; Schmitt et al., 2007; Bailey and Hallett, 2009; Smith et al., 2015). Bailey et al. (2004) found that hollowness appears at relatively high supersaturations of 50% and the depth of hollowness increases with increasing supersaturation. The hollowness generally appears to be conical (Heymsfield et al., 2002), but step-wise hollowness is also reported (Smith et al., 2015). Other observed crystals imperfections include air bubbles and soot-inclusions (e.g., Hong and Minnis, 2015; Panetta et al., 2016).

3 Ice crystal optical properties

For the interpretation of ice cloud remote sensing observations, appropriate optical properties of ice crystals are essential. Because ice crystals have non-spherical, complex structures and are generally much larger than solar wavelengths, exact methods for the calculation of optical properties, such as Lorenz–Mie theory (Mie, 1908) or the T-matrix approach (Mishchenko, 1991), are not suitable. Commonly, ice optical properties are approximated using geometric optics (GO) calculations, sometimes in combination with other methods. Already in the 17th century, GO principles were applied by Edme Mariotte and others to explain ice cloud halos. Modern applications are based on Monte Carlo ray tracing techniques that combine calculated paths of a large, finite number of light rays through the particle of interest assuming random orientations of the incoming ray. Early implementations of ray tracing were presented by Jacobowitz (1971) and Wendling et al. (1979), but more versatile computer codes that can be applied to complex particles and take into account light polarization are provided by Takano and Liou (1989) and Macke (1993) and are still much used today with some modifications. Although conventional GO has several shortcomings, mostly these issues are limited to its application to small and pristine particles with smooth surfaces (Bi et al., 2014; Yang et al., 2015). A comprehensive review of optical property calculations using conventional and modified geometric optics and other methods is given by Yang et al. (2015). Here, we aim to summarize the optical properties that are needed for the simulation of remote sensing data and to give a brief review of the dependency of optical properties on particle shape characteristics.

3.1 Definitions of optical properties

In order to solve the radiative transfer problem in the case of an ice cloud, the cloud layer optical thickness, single scattering albedo and phase matrix are needed (van de Hulst, 1957). The dimensionless optical thickness τ of a uniform ice cloud layer

of thickness ΔZ is given by

$$\tau = \Delta Z \, N_{\mathrm{tot}} \, \overline{\sigma_e} \tag{3}$$

where N_{tot} is the total number concentration of ice crystals and $\overline{\sigma_e}$ is the mean ice crystal extinction cross section. The extinction cross section for individual crystals can be written as a combination of absorption σ_a and scattering σ_s cross sections, i.e.

$$\sigma_e = \sigma_a + \sigma_s. \tag{4}$$

The fraction of light that is scattered rather than absorbed is given by the single scattering albedo ω defined as

$$\omega = \frac{\sigma_s}{\sigma_e}. \tag{5}$$

The extinction cross section of an ice crystal is largely determined by the projected area A_p of the ice crystal, i.e.,

$$\sigma_e = Q_e \, A_p, \tag{6}$$

where Q_e is the extinction efficiency. The projected area is defined as the crystal's average projection when an infinite number of random orientations are applied (Macke, 1993). For convex particles, A_p is equal to the total surface area divided by 4 (Vouk, 1948), while for particles with concave parts the projected area can be calculated using a Monte Carlo approach (Macke, 1993). In the conventional GO approximation, Q_e is 2 by definition (Berg et al., 2011), but actual values depend on particle size and shape (Yang et al., 2015). For particles with sizes comparable to the considered wavelength, ray interference leads to oscillations of Q_e around 2 that decrease in strength with increasing particle size. For particles much smaller than the wavelength, Q_e strongly decreases as it enters the Rayleigh scattering regime. Note however that generally the extinction coefficient is not very relevant for most remote sensing applications as the optical thickness is generally retrieved directly. However, the extinction coefficient is important for radiative transfer calculations based on model results (e.g., van Diedenhoven et al., 2012b; Bi et al., 2014; Baran et al., 2016).

The intensity and polarization state of light can be described by the Stokes vector $\mathbf{S} = (I, Q, U, V)$, where I is the total intensity, Q and U describe the linear polarization state and V describes the circular polarization state (van de Hulst, 1957). For each scattering event on randomly oriented ice crystals, the alteration of propagation direction and polarization state of incoming light is described by the symmetric phase matrix $\mathbf{P}$, which can be defined through (van de Hulst, 1957).

$$\begin{pmatrix} I_{\mathrm{s}} \\ Q_{\mathrm{s}} \\ U_{\mathrm{s}} \\ V_{\mathrm{s}} \end{pmatrix} = \frac{\sigma_s}{4\pi r^2} \begin{pmatrix} P_{11} & P_{12} & 0 & 0 \\ P_{12} & P_{22} & 0 & 0 \\ 0 & & P_{33} & -P_{34} \\ 0 & 0 & P_{34} & P_{44} \end{pmatrix} \begin{pmatrix} I_{\mathrm{in}} \\ Q_{\mathrm{in}} \\ U_{\mathrm{in}} \\ V_{\mathrm{in}} \end{pmatrix}, \tag{7}$$

where subscript "in" denotes the incoming Stokes vector, while "s" denotes the Stokes vector after scattering. Furthermore, r is the distance between the particle and the location at which $\mathbf{S_s}$ is evaluated. Note that all elements are a function of scattering

angle Θ. The first element of the phase matrix P_{11} is referred to as the scattering phase function and is the only element to be considered when polarization is ignored. The other elements describe the alteration of the light's polarization state at each scattering event. For example, the P_{12} element determines the linear polarization of light after one scattering event for incoming unpolarized light. The degree of linear polarization (DoLP) is given by P_{12}/P_{11}. Circular polarization can usually be ignored (Stamnes et al., 2016), but is relevant for lidars emitting circular polarized light (e.g., van Diedenhoven et al., 2009).

In the geometrics optics regime, the total scattering phase function includes contributions from refraction into and out of the particle and internal reflections and contributions from diffraction (Macke et al., 1996b), viz.

$$P_{11}(\Theta) = \frac{1}{2\omega}\Big[(2\omega - 1)P_{\mathrm{RT}}(\Theta) + P_{\mathrm{dif}}(\Theta)\Big], \tag{8}$$

where P_{dif} and P_{RT} are the contributions by diffraction and internal refraction and reflections, respectively. For radiative transfer applications that aim to approximate the upward and downward fluxes of light, e.g., so-called two-stream applications (Coakley and Chylek, 1975), the full phase function is not needed and only its first moment, the asymmetry parameter g, is considered. The asymmetry parameter is defined as

$$g = \int_0^\pi P_{\mathrm{tot}}(\Theta)\cos(\Theta)\sin(\Theta)\mathrm{d}\Theta. \tag{9}$$

The reflection of an ice cloud layer at a given wavelength and scattering geometry is primarily determined by the optical thickness, single scattering albedo and asymmetry parameter of the ice crystals. The detailed shape of the phase function is of second order importance.

The optical properties of single ice particles can be calculated using GO or other methods (Yang et al., 2015). Real ice clouds obviously consist of numerous ice crystals that have certain distributions of sizes and shapes. Recipes for integrating optical properties over such distributions are given by Baum et al. (2005).

3.2 Dependence of optical properties on crystal shape

The optical properties of ice depend on wavelength and ice size, shape and orientation. Here, we limit the discussion to randomly orientated crystals. Although horizontally oriented crystals are often present in clouds, it is estimated that their numbers are small and their influence on the integrated cloud properties is generally minimal (Bréon and Dubrulle, 2004; Zhou et al., 2012). Furthermore, essentially all radiative transfer and remote sensing applications are practically limited to randomly oriented particles.

The extinction efficiency mainly depends on the particle size parameter. It is commonly assumed that errors due to the GO approximations (i.e., $Q_e = 2$) are sufficiently small for most applications for particles with a size parameter greater than 100 (Baran, 2009; Bi et al., 2014). Following Bryant and Latimer (1969), here the size parameter χ at wavelength λ is defined as

$$\chi = (m_r - 1)\frac{2\pi}{\lambda}\frac{V}{A_p}, \tag{10}$$

where V is the volume of the particle and m_r is the real part of the refractive index of ice. This definition of size parameter depends on the volume-to-area ratio of the crystals. Confusingly, various other definitions of the size parameter that depend on,

e.g., maximum diameters or the radius of an equivalent-area sphere, are used in the available literature (e.g., Wyser and Yang, 1998; Zakharova and Mishchenko, 2000; Um et al., 2015). Bryant and Latimer (1969) showed that Q_e is a function of χ with a minimal dependency on shape and refractive index when the size parameter is defined as in Eq. 10. Occasionally ice extinction efficiencies are shown to be seemingly substantially dependent on shape, but at least part of the shape-dependency of the ice extinction efficiency reported in the literature is caused by using a definition of size parameter other than Eq. 10 (e.g., in Zakharova and Mishchenko, 2000; Yang et al., 2013; Liu et al., 2014; Um and McFarquhar, 2015). For example, extinction efficiencies presented as a function of maximum dimensions for different shapes may show functional differences, but the differences will be small if extinction efficiencies are instead presented as a function of the size parameter defined as by Eq. 10 (cf. Wyser and Yang, 1998).

The influence of particle shape on single scattering albedo is also limited (Wyser and Yang, 1998; Key et al., 2002; van Diedenhoven et al 2014a) since it mainly depends on the absorption size parameter as defined by van Diedenhoven et al. (2014a), i.e.,

$$\chi_{abs} = \frac{m_i V}{\lambda A_p}, \tag{11}$$

where m_i is the imaginary part of the refractive index. For a distribution of ice crystals, the integrated single scattering albedo at a given wavelength is mainly determined by the particle size distribution effective radius defined as

$$R_{\mathrm{eff}} = \frac{3}{4}\frac{V_{\mathrm{tot}}}{A_{\mathrm{tot}}}, \tag{12}$$

where V_{tot} and A_{tot} are the total volume and projected area of all particles in the cloud volume (Baum et al., 2005). This dominant influence of size, rather than shape, on the single scattering albedo make measurements that depend on the single scattering albedo, i.e. at shortwave infrared wavelengths, very suitable in retrieving particle effective radius (Nakajima and King, 1990).

In turn, the ice crystal scattering phase matrix is largely determined by particle shape, rather than size, especially at solar wavelengths where ice absorption is minimal. In fact, in the GO approximation and at non-absorbing wavelengths, the ray tracing part of the phase matrix is scale invariant by definition. Scattering phase matrices for crystals with size parameters smaller than about 100 do feature substantial size dependencies that are not accurately modeled by classical GO but these can be approximated by corrections to GO and/or by other techniques (Yang et al., 2015). However, most cross-sectional area is generally contributed by natural crystals larger than this limit when evaluated at solar wavelengths (Baran, 2009). As can be inferred from Eq. 8, the phase function is also affected by the single scattering albedo for non-absorbing wavelengths. Confusingly, substantial size-dependencies of scattering phase matrices for large particles at non-absorbing wavelengths are frequently presented in publications (e.g., Key et al., 2002; Baum et al., 2011, 2014). However, these variations of the phase matrices with size mostly stem from the assumed crystal geometries (e.g., the aspect ratios of ice crystal components) that depend on size. Although geometries might be expected to change with size for natural ice crystals, it is important to separate the dependence of optical properties on size from their dependence on crystal shape when considering the remote sensing of crystal shape. The strong dependence on shape of ice phase matrix elements at solar wavelengths and the minimal dependence on size are exploited by the methods to remotely sense information about ice shape using signatures in the scattered light, as discussed in section 4.

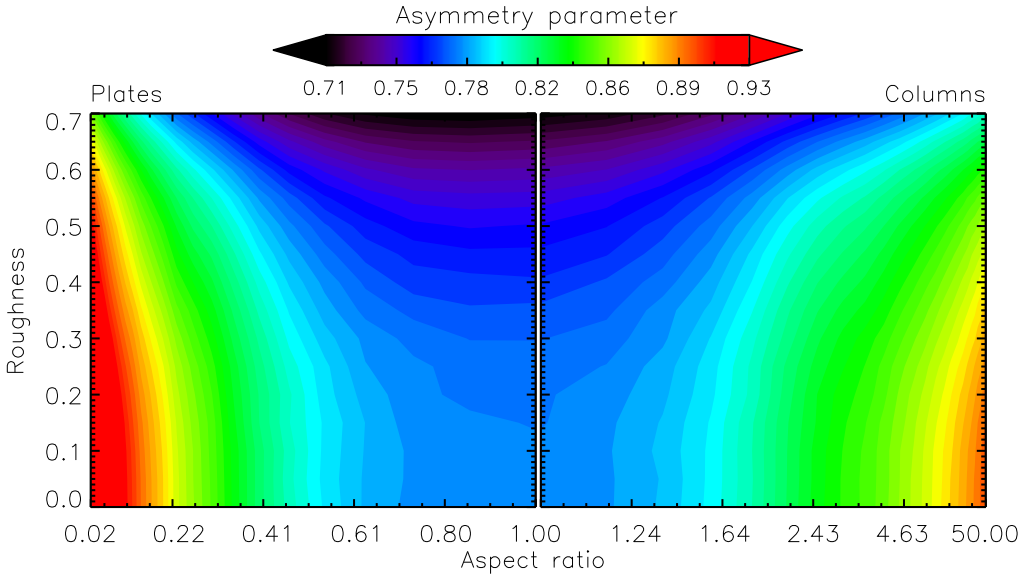

Figure 3. Asymmetry parameter of hexagonal prisms at a wavelength of 865 nm as a function of aspect ratio (x-axis) and roughness parameter (y-axis). Figure reproduced from van Diedenhoven et al. (2012a)

Thus, out of the fundamental optical properties, only scattering phase matrices are substantially dependent on shape. For the purpose of remote sensing of ice crystal shapes, it is important to determine to which shape characteristics the phase matrix is particularly sensitive. Early applications of ray tracing calculations already determined that the phase matrix of single hexagonal prisms show a strong dependence on their aspect ratio (e.g, Macke et al., 1996b). For example, the dependence of the asymmetry parameter at a wavelength of 865 nm on the aspect ratio hexagonal prisms is shown in Fig. 3. This figure also depicts the dependence of the asymmetry parameter on crystal surface roughness, as discussed later. As seen in Fig. 3, the asymmetry parameter is lowest for crystals with an aspect ratio near unity. Also the increase of asymmetry paramneter with aspect ratio is rather symmetric for plates and columns, implying that asymmetry parameter is largely determined by the aspect ratio $\alpha_{<1}$ as defined by Eq. 2 (van Diedenhoven et al., 2016a). Asymmetry parameters increase with aspect ratio owing to the increase of parallel surface areas leading to greater probability of light passing through the particle with low orders of refraction + reflection and a minimal change of direction (Yang and Fu, 2009). For the same reason, the increase of asymmetry parameter with decreasing aspect ratio $\alpha_{<1}$ is slightly weaker for columns than for plates owing to the larger parallel surfaces of plates (cf. Macke et al., 1996b; Yang and Fu, 2009). Examples of phase functions and the degree of linear polarization for hexagonal ice prism with varying aspect ratios and for various complex ice habits are shown in Figs. 4 and 5, respectively. The applied size distributions are described by van Diedenhoven et al. (2012a). From right panels in Figs. 4 and 5, one is tempted to conclude that ice optical properties strongly depend on the polycrystalline structure or habit. However, on closer inspection, the variation of phase function between different habits is mostly caused by the variation of the aspect ratio of

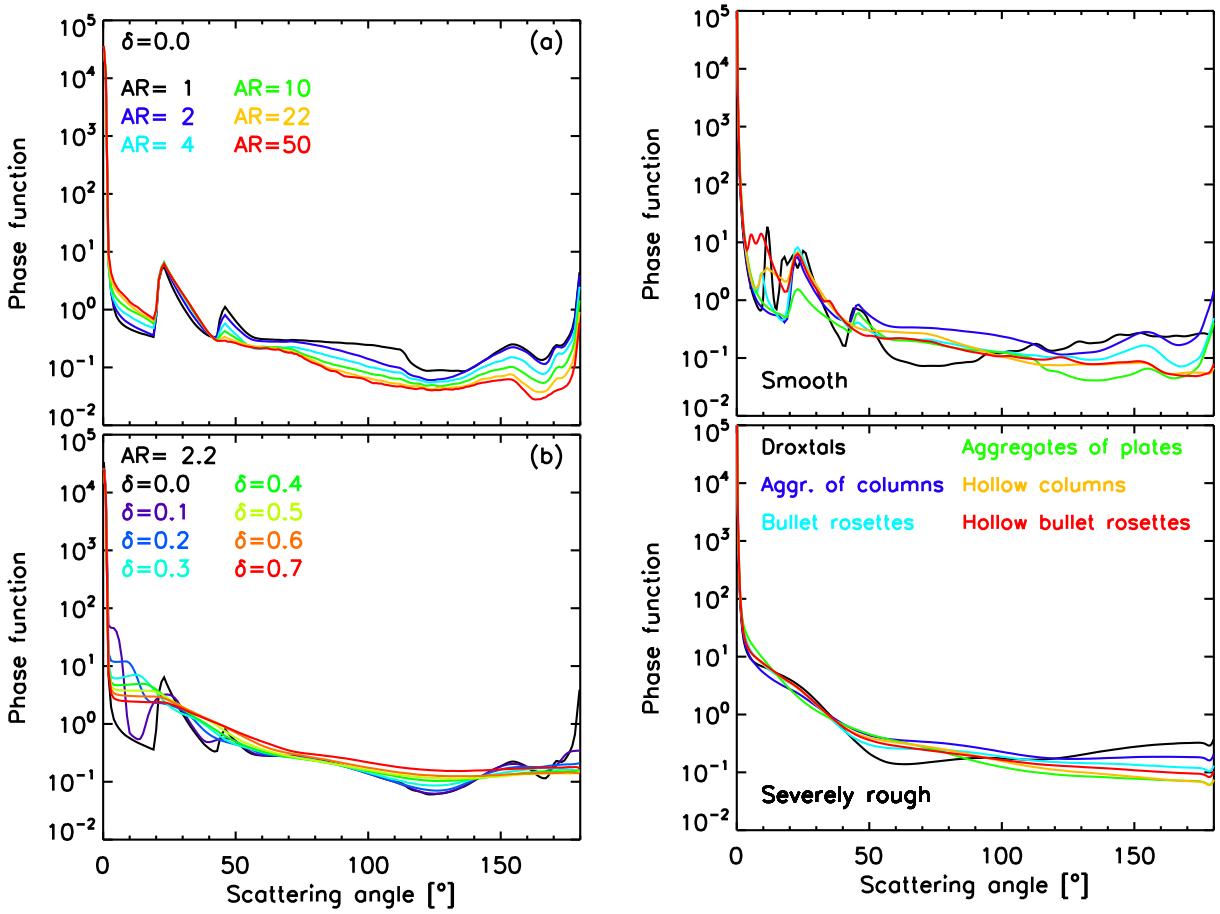

Figure 4. Phase functions of hexagonal columns with varying aspect ratios (AR, top left) and roughness parameters (lower left) and phase functions of complex crystals (Yang et al., 2015) with smooth (upper right) and severely roughneded ($\sigma = 0.5$, lower right) surfaces.

their components. For example, aggregates of columns have components with an average aspect ratio of 1.5 (Fu, 2007) and their phase matrix elements show resemblances with compact hexagonal columns (see Figs. 4 and 5), while bullet rosettes have thinner components and their phase matrices are similar to those of thin columns. Moreover, as was recognized by many authors (e.g., Iaquinta et al., 1995; Um and McFarquhar, 2007, 2009; Fu, 2007; Baran, 2009; van Diedenhoven et al., 2012a, 2014a), the phase function of an ice crystal consisting of multiple, identical hexagonal components largely resembles the phase function of the individual single components. Comparisons of phase functions of complex crystals and their components are shown previously for bullet rosettes and their aggregates (Iaquinta et al., 1995; Um and McFarquhar, 2007) and aggregates of plates (Baran, 2009; Um and McFarquhar, 2009) and columns (Baran, 2009). For various crystal habits, Fu (2007) showed that the asymmetry parameters of the complex crystals are approximated to within about 0.01 by the asymmetry parameters

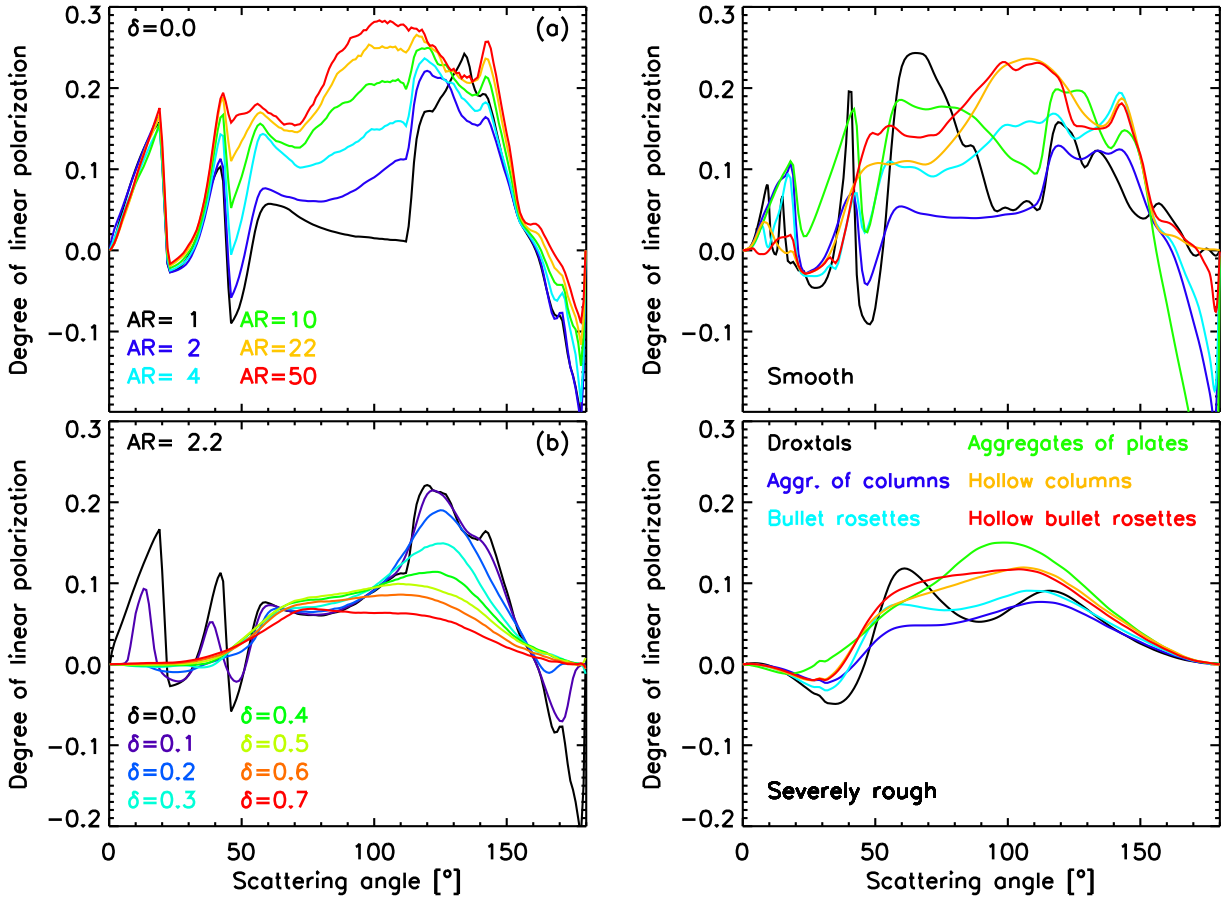

Figure 5. Same as Fig. 4 but for the degree of linear polarization.

of their individual components. Um and McFarquhar (2007) showed that the asymmetry parameter of individual bullets at visible wavelengths are about 0.01 larger than rosettes with 6 arms, and about 0.02 larger than an aggregate of bullet rosettes consisting of 18 components. For aggregates of plates, Um and McFarquhar (2009) showed that the asymmetry parameter at visible wavelengths decreases with roughly 0.01 for every 5 plates attached to an aggregate, although the decrease was found to be non-monotonic. Furthermore, they found that differences between asymmetry parameters of aggregates of plates and those of the component plates increase as the distances between the centres of mass of the plates within the aggregates decrease. Essentially, increasing the compactness of aggregate of plates leads to stacking of the plates and finally to morphing into a thicker single plate and hence to a lower asymmetry parameter. To put the sensitivity of the asymmetry parameter to aggregation into perspective, a small change in the aspect ratio of a single plate, from 0.6 to 0.5, increases the asymmetry parameter at a wavelength of 550 nm by 0.01, i.e., from 0.79 to 0.80. (Here the parameterization of van Diedenhoven et al. (2014a) is used to calculate the asymmetry parameter.) Thus, although the larger-scale structure of such complex particles

influences their single-scattering properties, the influence of natural variations in aspect ratios of crystal components may be expected to be greater.

As discussed in section 2.3, aside from general shape of ice crystals and the aspect ratios of their components, microscale structures on the crystal surfaces are of importance for optical properties. In order to compute the optical properties of a given ice crystal, an idealized definition of its facets is needed. However, the computational effort sharply increases as the number of facets required to define a particle with microscale surface roughness increases (Liu et al., 2013). Moreover, these complex or rough particles are determined by stochastic processes and all particles in a cloud volume essentially have unique complexity or roughness structures. To calculate the optical properties of such collections of particles, basically the optical properties of all many random members have to be determined and then appropriately averaged. Since this is impractical, stochastic approaches to approximate the effects of particle roughening have been developed. A commonly used method is based on the work of Peltoniemi et al. (1989), Macke et al. (1996b) and Yang and Liou (1998) and takes crystal roughness of ice crystals into account in a statistical manner by perturbing the normal of the crystal facet surface from its nominal orientation by an angle that, for each interaction with a ray, is varied randomly with a given distribution. This was found to be an effective and accurate treatment of the effects of surface roughness on ice crystal scattering properties (Liu et al., 2013). Practically, codes that use this approach (Macke et al., 1996b; Yang and Liou, 1998; Shcherbakov et al., 2006) vary in the assumed distribution of facet tilt angles (Neshyba et al., 2013; Geogdzhayev and van Diedenhoven, 2016). For instance, the code by Macke et al. (1996b) varies the tilt angles randomly with uniform distribution between 0° and $\delta \cdot 90^\circ$, where δ is referred to as the roughness parameter. Yang and Liou (1998) and Shcherbakov et al. (2006) vary tilt angles according to Gaussian and Weibull distributions, respectively, where the mean tilt angle is determined by roughness parameter σ. However, Geogdzhayev and van Diedenhoven (2016) and Neshyba et al. (2013) showed that roughness parameters with these different definitions, for a given value, lead to rather similar phase functions and asymmetry parameters (i.e. $\delta \approx \sigma$). However, these roughness parameterizations currently need to be considered as merely effective methods to simulate the effects of roughness structures on the scattering matrices, since they are difficult to relate to physical characteristics of the structures observed on real ice crystals, although attempts have been made (Neshyba et al., 2013). Furthermore, Liu et al. (2014) have shown that the simulated effects of microscale roughness features and larger scale geometric irregularities of ice crystals are similar. Indeed, irregular crystals such as Koch fractals (Macke et al., 1996b) and Voronoi particles (Letu et al., 2016) have phase matrices similar to rough hexagonal prisms. Increasing the number of impurities within ice crystals also has a similar effect (Macke et al., 1996a; Hong and Minnis, 2015; Panetta et al., 2016). Thus, the roughness parameterization can be interpreted as representing the randomization of reflection and refraction on and in the particles caused by any of such deviations from pristine, solid, smooth crystals. Since the roughness parameter reflects more than just roughness structures, some authors prefer the term "distortion parameter" instead. Using the definition of roughness of Macke et al. (1996b), Fig. 3 shows the dependence of the asymmetry parameter on roughness and aspect ratio, while the bottom left panel of Figs. 4 and 5 show the variation of phase functions and degree of linear polarization, respectively, on roughness for columns. Also, the bottom right panels of Figs. 4 and 5 show the phase functions and the degree of linear polarization, respectively, of severely roughened complex particles ($\sigma = 0.5$). Angular features in the phase functions and degree of linear polarization functions are smoothed out as roughness increases. Most notable, the halos are

diminished as roughness increases and asymmetry parameters systematically decrease with roughness (cf. Yang et al., 2008a; van Diedenhoven, 2014; van Diedenhoven et al., 2014a; Geogdzhayev and van Diedenhoven, 2016).

Another property of ice crystals that can have substantial impact of scattering properties is the presence of hollow crystal endings, or cavities (Schmitt et al., 2007; Yang et al., 2008b; Smith et al., 2015). Generally, asymmetry parameters increase as cavity depth increases, albeit this increase becomes smaller for crystals with aspect ratios increasingly deviating from unity (Schmitt et al., 2007). As can be seen in Fig. 4 (right panels), the hollow structures increase the scattering phase function values at scattering angles smaller than 20 degrees, but decrease values at side- and backscattering angles of 60 to 180 degrees (cf. Schmitt et al., 2007; Yang et al., 2008b). One way to interpret the observed influence of hollowness on columns is that, since the walls of the hollow parts of the crystals are thin, these essentially resemble columns with high aspect ratios, leading to an increased asymmetry parameter (van Diedenhoven et al., 2012a). This interpretation is also supported by the resemblance of phase functions and degree of linear polarization of hollow particles to those of columns with large aspect ratios seen in Figs. 4 and 5.

In summary, the most important features of ice particle shape influencing their optical properties are the aspect ratios of the crystals or the components of complex crystals as well as the microscale surface roughness, distortion or hollowness. The larger scale polycrystaline structure of the ice crystal is of lesser importance. Thus, the different characteristics of ice particle shape can be grouped in order of importance for the scattering properties as follows:

1. Aspect ratios of simple crystals or components of complex crystals;
2. Microscale structure, surface roughness, distortion, impurities or cavities;
3. Polycrystalline structure or habit.

These crystal shape characteristics are relevant targets for the remote sensing techniques described in the next section.

As discussed in section 2, myriads of shapes are found in real cloud volumes. Moreover, the aspect ratios and roughness levels may be expected to vary per particle (Um et al., 2015; Fridlind et al., 2016; Schnaiter et al., 2016). However, most publications about optical properties of ice crystals and remote sensing of ice crystal shapes consider calculations for individual crystals with a particular shape rather than mixtures of crystals with large variations in shapes, aspect ratios and roughness levels. Various habit mixtures have been presented (e.g., Baum et al., 2005, 2011; Baran and C.-Labonnote, 2007) but these usually contain just a handful of ice shapes. Furthermore, remote sensing applications generally aim to find a single shape or simple mixture that fits the measurements best. The question arises how to interpret remote sensing results that conclude one crystal shape or a limited mixture to be consistent with the measurements. In other words, which part of the ensemble is represented by the single inferred crystal shape? In order to estimate the asymmetry parameter of an ensemble of hexagonal ice crystals with a distribution of aspect ratios, Fu (2007) defined an ensemble-average aspect ratio as the average aspect ratio weighted by the orientation-averaged projected area of the crystals in the distribution. van Diedenhoven et al. (2016a) showed that the definition of aspect ratio limiting the values below unity for both plates and columns (i.e., Eq. 2) needs to be used in order for an ensemble-average aspect ratio to adequately represent the optical properties of the ensemble. Furthermore, they showed that even for

ensembles containing both columns and plates, the ensemble asymmetry parameters are generally represented consistently by a single crystal with an aspect ratio equal to the ensemble average, especially if geometrical averaging is used. Tests on mixtures of plates and columns yielded root-mean-squared differences between ensemble-average asymmetry parameters and those calculated from ensemble-average aspect ratios were 0.006. Furthermore, van Diedenhoven et al. (2016a) showed that effective asymmetry parameters based on arithmetic averages of roughness parameters are also largely consistent with ensemble-average asymmetry parameters. As discussed by Fu (2007) and van Diedenhoven et al. (2016a), these conclusions are likely qualitatively applicable to ensembles of more complex structures such as aggregates of columns, aggregates of plates and bullet rosettes with a range of aspect ratios of their components, as well as to internal mixtures of plate-like and column-like components, such as asymmetric bullet rosettes, aggregates of varying plates and/or columns or plate-capped columns. Thus, the conclusions by Fu (2007) and van Diedenhoven et al. (2016a) suggest that shapes inferred from remote sensing applications represent an area-weighted ensemble average of the ice crystals in the observed cloud volume. Further discussion on this is included in section 4.2.4.

In summary, it is practically impossible to consider all geometries of ice crystals formed in natural ice clouds for remote sensing applications. Any ice model used for remote sensing purposes will be a highly idealized simplification of natural ice crystals. Often, crystal shapes that are found to match observations are presented merely as "radiative equivalent effective shapes" (e.g., McFarlane and Marchand, 2008; Cole et al., 2013), and no direct relation between the inferred shape and the ice crystal shapes in the observed clouds is claimed. However, using idealized models, it is still possible to infer useful information about shape characteristics of natural ice crystals in clouds. Here, a famous quote from the late George Box is fitting, namely that "essentially, all models are wrong, but some are useful" (Box and Draper, 1987). In order to infer information about the variation of ice crystal shape in ice clouds, a set of ice models is needed that systematically varies the physical and scattering properties and is able to fit the full range of available remote sensing observations. George Box provides further inspiration by stating that "since all models are wrong, the scientist cannot obtain a ‘correct’ one by excessive elaboration. On the contrary, following William of Occam [she/]he should seek an economical description of natural phenomena" (Box, 1976). Following such wisdom, one can conclude that for remote sensing it may be advised to focus on the variation of the ice shape characteristics that are mostly determining the radiative properties as listed above, i.e., component aspect ratios and microscale structure, and less on crystal habits. Note that shape characteristics such as aspect ratios, roughness levels and cavity depths are quantitative parameters that suit systematical variation in contrast to ’habit’. Focusing on such shape parameters provides a "economical description" and reduces the remote sensing problem substantially to quantifying these parameters without considering the virtually infinite number of possible large-scale shapes. Based on the equivalence of scattering properties of complex crystals and their components, as discussed above, such inferred parameters, e.g., aspect ratios and roughness parameters, represent the averaged properties of the components of the crystals in the observed ice clouds. Given the variation of ice crystals observed and the myriad of conditions in which ice crystals form and evolve, we can assume that values of aspect ratios and roughness levels occur continuously over rather large ranges, which need to be spanned by the models considered for remote sensing applications to infer ice crystal shapes.

4 Remote sensing of ice crystal shapes

Essentially two different observational approaches have particular potential for inferring information about particle shape, namely active lidar observations and passive multi-directional measurements of total and/or polarized reflectances. Here, these approaches are discussed separately in sections 4.1 and 4.2.

4.1 Lidar measurements

Lidars (i.e., laser radars) probe clouds by emitting laser beam pulses and measuring the power of the returned signals (Weitkamp, 2005). By measuring the delay between the emitted and detected beams, the distance between the lidar and the cloud volume on which the beam was scattered back can be determined, resulting in height-resolved information. When the emitted beam is polarized and the polarization state of the detected signal is measured, the depolarization of the beam caused by backscattering on particles can be measured. The altitude-dependent linear depolarization ratio δ_l of the returned signal is usually defined as (Schotland et al., 1971)

$$\delta_l(z) = \frac{\beta_\perp(z)}{\beta_\parallel(z)}, \tag{13}$$

where β is the backscattering cross sections in the planes of polarization perpendicular ($\perp$) and parallel ($\parallel$) to the laser's reference plane. In Eq. 13 it is assumed that atmospheric extinction is independent of the polarization state of the propagating radiation. Other definitions for lidar depolarization are discussed by Gimmestad (2008).

Since lidar signals are mainly determined by singly scattering light, the depolarization of a lidar signal returned from a cloud layer can be simulated in a straight forward manner from the assumed scattering phase matrix, namely by

$$\delta_l(z) = \frac{P_{11}(180°) - P_{22}(180°)}{P_{11}(180°) + P_{22}(180°)}. \tag{14}$$

Lorenz-Mie theory applied to spherical particles shows that no depolarization is caused by single back-scattering on purely spherical cloud droplets, although multiple scattering on liquid cloud drops can lead to some depolarization of the lidar signal (Sassen and Petrilla, 1986; Hu et al., 2001). However, single back-scattering of the laser light on non-spherical particles such as spheroids or hexagonal prisms leads to substantial depolarization of the signal that is largely dependent on particle shape.

The first ground-based lidar depolarization measurements of clouds were reported by Schotland et al. (1971) and many polarized ground-based lidars are deployed world-wide today. The satellite-based Cloud-Aerosol Lidar with Orthogonal Polarization (CALIOP) on the Cloud-Aerosol Lidar and Infrared Pathfinder Satellite Observation (CALIPSO) platform (Winker et al., 2007), launched in 2006, is particularly relevant for ice cloud studies as it is providing global statistics and observes cirrus otherwise obscured by lower lying liquid clouds when viewed from the surface. Similar statistics are expected from the Atmospheric Lidar (ATLID) on the Earthcare platform to be launched in 2018 (Lefebvre et al., 2016). Furthermore, the cloud physics lidar (CPL) has been providing a wealth of data since the year 2000 while mounted on the high altitude NASA ER-2 aircraft during many field campaigns targeting clouds (Yorks et al., 2011). General conclusions about the depolarization measured by such lidars is that the depolarization ratio in ice clouds typically range from 0.2 to 0.6, and generally increases with increasing

cloud height or decreasing temperature (Sassen and Benson, 2001; Reichardt et al., 2002; Noel et al., 2004; Sassen and Zhu, 2009; Yorks et al., 2011; Baum et al., 2011; Sassen et al., 2012). Furthermore, CALIOP statistics presented by Sassen et al. (2012) show a globally, vertically and yearly averaged ice cloud depolarization ratio of 0.37 and generally lower values at higher latitudes. In addition, Martins et al. (2011) found no significant variations in depolarization ratios for ice clouds in relation to updraft strength or horizontal windspeed. Note that the depolarization ratios quoted here reflect the values measured at an off-nadir angle, since horizontally orientated ice crystals strongly decrease depolarization measured at direct nadir owing to specular reflection on the crystal surfaces (Del Guasta et al., 2006; Zhou et al., 2012; Sassen et al., 2012).

Although the variation of depolarization ratios in ice clouds at different altitudes, temperatures and latitudes are fairly well documented, a definite quantitative interpretation of the values in terms of ice crystals shape variations is lacking. One interpretation is offered by Noel et al. (2002) who showed that the simulated depolarization ratio of single hexagonal prisms depends on their aspect ratio. As also shown by Yang and Fu (2009), the simulated depolarization ratio of hexagonal crystals with smooth surfaces is about 0.2 for thin plates, oscillating between 0.3 and 0.4 for thicker plates and about 0.4–0.6 for compact particles and columns. Based on this relation between depolarization ratio and aspect ratio, Noel et al. (2004) concluded that the depolarization ratios observed by the CPL during the CRYSTAL-FACE campaign conducted near Florida in 2002 are consistent with a dominance of compact or 'irregular' crystals and an increasing contribution by plate-like crystals with increasing cloud top temperature. Measurements on ice crystals grown in the laboratory presented by Amsler et al. (2009) and Abdelmonem et al. (2011) seem to support this quantitative interpretation of depolarization ratios, although modeled depolarization ratios were found to be generally larger than the measured ones. However, as discussed in section 2, most crystals observed in situ have more complex, aggregated shapes than simple hexagonal prisms. Although large scale complexity generally has a weaker effect on the scattering phase matrix than aspect ratio, as discussed in section 3.2, it is unclear whether or how this complexity affects the depolarization ratios specifically (Reichardt et al., 2008). A fundamental problem for simulating lidar backscattering and depolarization on ice crystals is that the phase matrix computed based on geometric optics exhibits a singularity at the exact backscattering direction for randomly oriented crystals (Borovoi et al., 2005, 2014). Usually values for angles close to 180 degrees are used instead or they are extrapolated towards 180 degrees (e.g., Smith et al., 2016). Furthermore, the dependency of depolarization on aspect ratio presented previously by Noel et al. (2004) and others are based on solid crystals with smooth surfaces. Although calculations presented by Smith et al. (2016) suggest that the effects of crystal hollowness on lidar depolarization is generally small, reported estimates of the effects of surface roughness on lidar depolarization are inconclusive. Mostly, roughness or distortion of ice crystals is shown to lead to a decrease of depolarization (Del Guasta, 2001; Baum et al., 2010, 2011), although the opposite trend has been shown as well (Smith et al., 2016; Konoshonkin et al., 2016). Furthermore, rounded crystal shapes caused by crystal sublimation are sometimes associated with a decrease of depolarization (e.g., Martins et al., 2011), although increasing depolarization from sublimation is suggested by Schnaiter et al. (2012). Also, low depolarization in ice clouds are sometimes interpreted as caused by compact or 'quasi-spherical' particles (e.g., Choi et al., 2010). However, these associations may not be supported by observations and calculations of optical properties. For example, Mishchenko and Sassen (1998) showed that depolarization ratios of spheroids and deformed spheroids with aspect ratios close to unity are comparable with, or larger than, the values of hexagonal plates, even if such shapes can

be considered quasi-spherical. Sassen (1977) reported depolarization ratios above 0.5 for frozen rainwater drops with a regular spherical or spheroidal appearance. In contrast, recent work presented by Järvinen et al. (2016) and Schmitt et al. (2016) shows that sublimation of ice crystals can lead to smooth frozen droplets that have optical properties similar to spheres including near-zero depolarization ratios. Other factors complicating the interpretation of lidar depolarization values are the presence of oriented ice crystals (Del Guasta et al., 2006; Zhou et al., 2012) and the co-existence of ice crystals and liquid drops in mixed-phase clouds (Bourdages et al., 2009; van Diedenhoven et al., 2011)

In conclusion, systematic variations of lidar depolarization in clouds are observed, but their interpretation is currently inconclusive. As put by Sassen et al. (2012), "these [variations in depolarization ratios] must reflect the different ice particle shapes that depend on the cirrus cloud formation mechanism (e.g., convective-anvil, orographic, synoptic, etc.), or more specifically on the basic cloud-particle forming aerosol available for crystal formation and the microphysical effects of typical cloud updraft velocities." However, currently, interpretations of lidar depolarizations in ice clouds are more qualitative than quantitative. To quantitatively relate the measured depolarization ratios to microphysical properties of the ice crystals, more research is needed, including 1) further development of methods for calculating exact backscattering properties of complex ice crystals and crystals with randomly roughened surfaces; 2) investigations on the effects of crystal complexity on lidar depolarization; 3) further statistical studies on measured lidar depolarization ratios with co-located in situ ice crystal shape observations.

4.2 Multi-angular measurements

As shown in Figs. 4 and 5, the shapes of the scattering phase function and degree of polarization of ice crystals for visible wavelengths depend on the crystal shape. These angular variations in scattering phase function and degree of polarization lead to angular features in the total and polarized reflectances of ice clouds that can be observed by remote sensing instruments that make observations at multiple viewing angles per instrument footprint. Here, we first sumarize the techniques used to infer ice crystal shape from multi-angular total reflectances (section 4.2.1) and multi-angular polarized reflectances (section 4.2.2). Then some discussion about data selection and availability is offered in section 4.2.3 before summarizing results in section 4.2.4.

4.2.1 Multi-angular total reflectances

The measured reflectance of a cloud layer can be defined as

$$R(\mu_0, \mu, \Delta\phi) = \frac{\pi I(\mu_0, \mu, \Delta\phi)}{\mu_0 F_\odot}, \tag{15}$$

where μ_0 and μ are the cosine of the solar zenith angle and viewing angle, respectively, $F_\odot$ is the solar irradiance, and I is the radiance measured by an instrument. Since this definition refers to the reflectance of light irregardless the polarization state, it is commonly referred to as "total reflectance".

Ice crystal shape can be inferred from total reflectances because angular features in the single scattering phase function of ice crystals, as seen in Fig. 4 for example, are preserved in the directional measurements. The directional reflectance of singly scattered light is determined by the phase function (van de Hulst, 1957). Because of the large extinction in cloud tops, however,

singly scattered light emerging from the cloud is only a small fraction of the total reflection, adding a weak signal of directionality to the measured total reflectances. As discussed in section 3, the magnitude of the total reflectance of an ice cloud is mostly determined by its optical thickness and the asymmetry parameter of the scattering phase function (Coakley and Chylek, 1975). One might expect that multiply scattered light emerging from a cloud is fully isotropic. However, as explained by Zhang et al. (2009), at any scattering event, the highly peaked phase functions of ice crystals lead to a large portion of the rays scattered forward without a substantial change in direction. Thus, a likely path for light rays is one where one or more forward scattering events are followed by a single side-ward scattering event, which is then subsequently followed by one or more forward scattering events again before light emerges from the cloud and is measured by an instrument. Although such paths describe multiply scattered light, the angular features in the scattering matrix of ice crystals are also preserved in the directional reflectance measurements for these paths, similarly as for the singly scattered light. This effect enhances the signal to noise ratio and the information content of multi-directional total reflectance measurements for the use of retrieving ice crystals shape.

For a plane-parallel homogeneous cloud layer, its visible reflectance at a particular viewing geometry is fully determined by the scattering phase function and the optical thickness. Thus, when multi-directional measurements are available for a cloud layer, an optical thickness can be retrieved from each angular measurement assuming a particular phase function. If the assumed phase function is correct then the optical thickness retrieved at each angle would be exactly the same, i.e., the correct value. However, an incorrect phase function assumption leads to an angular dependence of the retrieved optical thickness. This angular variation of retrieved optical thickness, or spherical albedos derived from them (e.g., Doutriaux-Boucher et al., 2000), is the basis of methods to retrieve ice shapes from multi-angular total reflectances (e.g., Doutriaux-Boucher et al., 2000; McFarlane and Marchand, 2008). Generally, the angular variation of retrieved optical thicknesses or spherical albedos is determined for a selection of assumed crystal shapes and crystals leading to the smallest angular variations are presented as the most consistent with real ice crystals.

Examples of instruments that make measurements of total reflectances at multiple viewing angles per footprint are NASA's Multi-angle Imaging SpectroRadiometer (MISR, Diner et al., 2002) and ESA's Along-Track Scanning Radiometer 2 (ATSR-2) and the Advanced ATSR (AATSR) (Sayer et al., 2011). The ATSR-2 and AATSR instruments have nadir pointing cameras as well as one forward pointing camera observing each footprint. MISR has 9 cameras at nadir, forward and aft pointing angles. Also multi-angle polarimeters as discussed in section 4.2.2 measure total reflectances in addition to the polarized reflectances. Overlapping footprints of geostationary satellite imagers have also been used to create dual-view observations (Chepfer et al., 2002). Furthermore, global statistics of single-view imager data can be used to infer the angular variation of cloud reflectances (Zhang et al., 2009; Wang et al., 2014).

4.2.2 Multi-angular polarized reflectances

Similar to the definition of total reflectances (Eq. 15), polarized reflectances R_p are generally defined as

$$R_p(\mu_0, \mu, \Delta\phi) = \frac{\pi\sqrt{Q^2 + U^2}}{\mu_0 F_\odot}. \tag{16}$$

The dependency of Q and U on μ_0, μ and $\Delta\phi$ is omitted in Eq. 16 for clarity. Note that both Q and U are signed according to the orientation of the measured electromagnetic wave relative to a reference plane. This information about polarization direction is lost by the definition of Eq. 16, but can be analyzed separately (e.g., Sun et al., 2015) or a sign can be added to the polarized reflectances accordingly, as described by C.-Labonnote et al. (2001). Normalizations different from the one used in Eq. 16 are sometimes applied too (e.g., C.-Labonnote et al., 2001).

Ice crystals shape characteristics can be inferred from the polarized reflectances by matching the measured angular variation of polarized reflectances with values simulated using a radiative transfer model that includes multiple scattering and polarization. Since multiple scattering depolarizes light, polarized reflectances are dominated by singly scattered light and have pronounced angular dependencies that are determined by the polarization properties of the ice crystals, as shown in Fig. 5. Furthermore, for cloud optical thickness values above about 2–5 (depending on the asymmetry parameter of the phase functions), polarized reflectances do not depend on cloud optical thickness anymore (van Diedenhoven et al., 2012a), which is convenient when retrieving information about ice crystals shape in various thick cloud types. However, measuring the polarization state of reflected light is challenging, as per footprint and per viewing angle it requires a minimal set of three simultaneous observations at three well-determined polarization angles (Tyo et al., 2006).

Relevant multi-angular polarized reflectances from space were measured by the POLarization and Directionality of the Earth's Reflectances (POLDER) instruments (Deschamps et al., 1994; Fougnie et al., 2007). The POLDER imager acquired overlapping images at different orbital locations that yield observations for each given footprint at a maximum of 16 viewing angles (Fougnie et al., 2007). For the POLDER wavelength bands at 490, 670, and 865 nm, three acquisitions are performed through a polarizer oriented at -60°, 0°, and 60° relative to a given reference from which the Stokes parameters $[I,Q,U]$ are retrieved. In addition to an airborne version of the POLDER instrument (Chepfer et al., 1998), three satellite-based versions were deployed. The first two (POLDER-1 and POLDER-2) were mounted on the Advanced Earth Observing Satellite (ADEOS-1 and ADEOS-2, respectively), but both only lasted for about 6 months owing to platform failures. The third, mounted on the CNES/Myriade Polarization & Anisotropy of Reflectance for Atmospheric Sciences coupled with Observations from a Lidar (PARASOL) microsatellite, was highly successful and lasted for nearly 9 years, from 2004 to 2013. POLDER/PARASOL was part of NASA's afternoon train (A-train) constellation until 2010, allowing its data to be combined with that of Cloudsat, CALIPSO, MODIS and other A-train instruments. No multi-directional polarimeter other than POLDER has flown in space to date. Unfortunately, the launch of the Glory satellite carrying the Aerosol Polarimetry Sensor (APS, Mishchenko et al., 2007) failed in March 2011. Several airborne multi-angle polarimeters are regularly deployed during field campaigns, often on high altitude aircraft capable of flying sufficiently above ice clouds. The Research Scanning Polarimeter (RSP, Cairns et al., 2003) is an airborne version of the APS and provides simultaneous measurements of total and polarized reflectances in 9 spectral bands from the visible to the shortwave infrared. The RSP scans along track, providing measurements of each pixel at 152 different viewing angles at 0.8 degrees intervals. Other deployed airborne polarimeters include the Airborne Multi-angle Spectro Polarimetric Imager (AirMSPI, Diner et al., 2013) and Airborne Spectropolarimeter for Planetary EXploration (SPEX, Rietjens et al., 2015).

4.2.3 Data selection

For the remote sensing of ice crystal shape, employing relevant data selection criteria is crucial. Obviously, one important selection criteria is that ice clouds are selected without interference of liquid clouds. For studies on POLDER data, this is generally efficiently achieved by testing for rainbow features in polarized reflectances. However, as noted by, e.g, C.-Labonnote et al. (2001) and Cole et al. (2014) this generally filters out clouds with low optical thicknesses (below optical thickness 1–5). This inadvertent selection of thick clouds is often not noted by studies using POLDER data, although evidently statistics of POLDER polarized reflectances generally show saturated reflectances, which only occur at about optical depths of about 4–5 (Chepfer et al., 2001; van Diedenhoven et al., 2013). Since cirrus typically has an optical thickness below 4 (Rossow and Schiffer, 1999), this selection has the important implication that that most cirrus are not included in the studies on ice crystals shapes using POLDER data. Alternatively, collocated MODIS thermodynamical phase determination can be used to select ice-topped clouds. However, this cloud phase retrieval is shown to be less reliable for mixed-phase and multi-layered clouds (e.g., Riedi et al., 2010). Interference of liquid drops to the multi-angular total or polarized reflectances is expected to lead to spurious angular dependence of the measurements and thus to biases the retrievals of ice shape towards more pristine particles.

Since the simulations of ice optical properties and radiative transfer calculations generally assume random orientation of the ice crystals, Chepfer et al. (2001) and Sun et al. (2006) concluded that the POLDER data needs to be screened for the presence of oriented ice crystals. Specular reflection on oriented crystals is highly polarizing and leads to sharp angular peaks in the polarized reflectances at the specular reflection angles (Chepfer et al., 1998; Bréon and Dubrulle, 2004). This peak can be used to screen the data for particle orientation, but it requires measurements at and around the scattering angle associated with specular reflection for a given solar angle. As noted by Sun et al. (2006), this requirement excludes most data, especially for instruments with relatively low angular resolution such as POLDER. For example, Sun et al. (2006) noted that the stringent data selection criteria used in their study on POLDER data lead to only 0.37% of the 5-month POLDER dataset passing these criteria. However, analyzes of global POLDER data suggests that that the relative number of oriented crystals is generally low and that the typical effective contribution to particle area from oriented plates in clouds is smaller than 1% (Bréon and Dubrulle, 2004). Thus, the total and polarized reflectances from ice clouds outside of the specular reflection geometry are dominated by randomly oriented crystals, which implies that the screening for random orientation is not needed. It may be needed to remove data affected by sunglint on ocean surfaces (van Diedenhoven et al., 2013), although this will only be an issue for optically thin clouds that are generally already excluded from POLDER measurements.

As the crystal shape information is inferred from angular variations in total and polarized reflectances, the information content depends on the scattering angles that are sampled by the instrument. In turn, the sampled scattering angles are dependent on the solar zenith angle and thus on latitude when analyzing data from polar orbiting satellites. It is important to note that for the statistics on polarized reflectances derived from global POLDER measurements, data from higher latitudes contribute more towards the small scattering angles, while tropical clouds contribute more to the larger scattering angles (Buriez et al., 2001). This also implies that any latitudinal variations in retrieved ice model or roughness level may stem from the latitudinal

variation of available scattering angles and the sensitivity of the retrieval approaches to scattering angle range. Results from van Diedenhoven et al. (2012a, 2013) show that an angular range including samples between scattering angles of at least 120° and 150° is needed for ice crystal shape retrievals. However, the retrieval performance is shown to be rather insensitive to number of angles sampled within that range or to any reasonable random error or bias on the measurements (van Diedenhoven et al., 2012a).

4.2.4 Overview of results

An overview of the most notable studies on inferring ice crystal shape along with the targeted locations and the data used is given in Table 1. Some studies use total reflectances R, some use polarized reflectances R_p and some use both. Most studies analyze data averaged over time and space, while some infer crystal shapes from data at the instrument's pixel resolution. The table also lists a description of the dominating ice shape found by the particular studies. From this overview it is clear that most data are fitted best by crystals with roughness, impurities or other distortions. Some studies, especially early ones, did not include particle roughness or other distortions and their results should be treated with caution.

Table 1: Overview of studies on remote sensing of ice crystal shapes

Reference(s)	**Region or target**	**Data used**	**Dominating shapes**	**Notes**
Baran et al. (1998, 1999)	Tropical anvil, cirrus	ATSR-2 dual view	Koch fractals	No roughness or inclusions
Chepfer et al. (1998)	EUCREX'94 campaign, mid-lat. cirrus	Airborne POLDER R and R_p	Pristine thin plates, α= 0.05–0.1	No roughness or inclusions
Doutriaux-Boucher et al. (2000); C.-Labonnote et al. (2000, 2001)	Global ocean & land	POLDER-1 R and R_p	Columns with inclusions, α=5	
Chepfer et al. (2001)	Global ocean & land	Pixel level POLDER-1 R_p	Koch fractals and columns at low latitudes; Plates at high latitudes	No roughness or inclusions
Chepfer et al. (2002)	Continental USA	GOES West and East dual view	Compacts, columns, and bullet rosettes	No roughness or inclusions
Knap et al. (2005)	Global ocean	POLDER-2 R and R_p	Columns with inclusions or roughness, α = 2.5	
Knap et al. (2005)	Tropical anvil outflow	ATSR-2 dual view	Moderately roughened columns	
Sun et al. (2006)	Global ocean	Pixel level POLDER-1 R_p	Plates and hollow columns	Few rough particles considered
Baran and C.-Labonnote (2006)	Global ocean	POLDER-2 R and R_p	Rough crystals, $\delta = 0.4$	
McFarlane and Marchand (2008)	Southern Great Plains	Pixel level MISR+MODIS	Rough aggregate and bullet rosettes	
van Diedenhoven et al. (2012b)	TWP-ICE campaign	POLDER-PARASOL R_p	Rough plates: α=0.7 at T<-38°C; α=0.15 at T>-38°C	Only 2 plate aspect ratios considered

Table 1: (continued)

Reference(s)	Region or target	Data used	Dominating shapes	Notes
van Diedenhoven et al. (2013)	CRYSTAL-FACE campaign Florida	Pixel level RSP R_p	Rough compact and plate-like crystals	
Cole et al. (2013)	Global ocean	POLDER-PARASOL R and R_p	Rough habit mixture	
van Diedenhoven et al. (2014b)	TWP-ICE campaign	Pixel level POLDER-PARASOL R_p	Rough plates with δ=0.4–0.7	Properties vary with height and convective strength
Cole et al. (2014)	Global ocean	Pixel level POLDER-PARASOL R_p	Rough aggregate of columns	Roughness varies with latitude
Wang et al. (2014)	Global ocean & land	MODIS over optically thin cirrus.	Mixture of rough and smooth crystals	Differences between ocean and land
Baum et al. (2014)	Global ocean	POLDER-PARASOL R_p	Rough habit mixture	
Baran et al. (2015)	Off coast of Scotland	Pixel level POLDER-PARASOL R	Rough crystal mixtures	Data interpreted as roughness varying with humidity
Letu et al. (2016)	Global ocean	POLDER-PARASOL R	"Voronoi" habit	
Hioki et al. (2016)	Global ocean	Pixel level POLDER-PARASOL R_p	Rough aggregate of columns (only habit considered)	Unphysically large roughness parameters for 74% of data

Many of the studies listed in Table 1 aim to find ice crystal models that best represent globally averaged data. Some studies compare total reflectances with modeled reflectances in order to identify crystal shapes that lead to most realistic angular features on average (e.g., Doutriaux-Boucher et al., 2000). Studies on global polarized reflectances usually present observation density plots of the POLDER measurements as a function of scattering angles to which simulated polarized reflectances are compared (e.g., Knap et al., 2005; Baran and C.-Labonnote, 2006; Cole et al., 2013). These density plots represent the statistics of polarized reflectances observed at any specific scattering angle. The range of measured polarized reflectances can be assumed to stem from the natural variation in ice crystals shapes. It is generally concluded that the ice shapes that lead to simulated polarized reflectances that are closest to most observations at all of the scattering angles is a good model to represent natural ice clouds. However, it is important to note that almost all models included in such studies generally lead to simulated polarized reflectances that fall within the observation envelopes at most scattering angles. This implies that all such models could represent a subset of the measurements. For example, Cole et al. (2013) evaluate simulated polarized reflectances for habit mixtures with smooth or rough surfaces, as well several habits with severely rough surfaces (droxtal, solid 3D bullet rosette, hollow 3D bullet rosette, hollow column, solid column, plate, compact aggregate of columns, small spatial aggregate of plates, and large spatial aggregate of plates) and all simulations fall within the observation envelopes. The results of Baran and C.-Labonnote (2006) show that polarized reflectances simulated assuming smooth bullet rosettes and smooth chain-like aggregates of columns, as well as rough and distorted crystals, fall within the global statistics of measured polarized reflectances. In addition, the range of observed angular variations of total reflectances is also large in comparison to the variation in modeled angular features for different ice models (Doutriaux-Boucher et al., 2000; Baran and C.-Labonnote, 2006; Baran, 2009; Cole et al., 2013), again suggesting that many considered models may fit well to a subset of the measurements. Many such studies aim to select and test optical models for global retrievals of ice cloud optical thickness and effective radius and selecting a model that fit best to most of the globally averaged data is very much justified in this case. However, as pointed out by McFarlane and Marchand (2008) "using a featureless phase function will likely result in the correct scattering properties on average, however individual cases may have large errors." To avoid such biases, simultaneous retrievals of ice crystal shape and size can be employed on a pixel level (McFarlane and Marchand, 2008; van Diedenhoven et al., 2014b). For the purpose of collecting information about how ice crystal shape varies with, e.g., temperature, cloud type and atmospheric state, it is important to study the variation in ice shape and crystal roughness leading to the ranges of observed angular total and polarized relfectances.

Studies that focus on the variation of ice crystals shapes are presented by, e.g, Chepfer et al. (2001), Sun et al. (2006), Cole et al. (2014) and Baran et al. (2015). Analyzing global POLDER-1 data, Chepfer et al. (2001) concluded that "polycrystals" [i.e., Koch fractals (Macke et al., 1996b)] and hexagonal columns seem to dominant at low latitudes, whereas the hexagonal plates seems to occur more frequently at high latitudes. However, other than the Koch fractal, no other distorted or roughened crystals are included in that study. More recently, Cole et al. (2014) included 9 different shapes (Yang et al., 2015) and a mixture (Baum et al., 2011) with a large range of simulated roughness levels in their global study. They found that the aggregate of columns dominates at all latitudes and plates are the least representative of the POLDER-PARASOL polarized reflectances globally. Interestingly, particles with smooth surfaces (no or low roughness levels) were found to be more prevalent

at high latitudes, while severely rough crystals (σ=0.5) were observed most frequently in the Tropics. This suggests that, in general, ice phase functions and polarization functions have some more angular features in the high latitudes than at low latitudes, which may be consistent with the findings of Chepfer et al. (2001) that smooth hexagonal plates fit the POLDER-1 data more frequently at high latitudes than elsewhere. Few roughness parameter values $\sigma > 0.5$ were found by Cole et al. (2014). Somewhat in contrast with these results are the results of Hioki et al. (2016). Applying an algorithm based on empirical orthogonal function analysis of the modeled and measured POLDER-PARASOL polarized reflectances and assuming aggregates of columns with varying roughness, Hioki et al. (2016) found roughness values varying with latitude, but they obtained $\sigma > 1$ for most data, which is unrealistically large. They conclude that the unexpected results indicate that the roughness retrieval is sensitive to an assumed particle shape, although the same aggregates of columns model with $\sigma \leq 0.5$ is found to be matching the data well by Cole et al. (2014). The results by Sun et al. (2006), analyzing global POLDER-1 data, also appear to be in conflict with the studies by Chepfer et al. (2001) and Cole et al. (2014) and arguably every other study listed in Table 1, since rough particles were found to fit virtually none of the measurements and smooth plates and hollow columns were inferred from the data most frequently. Smooth plates and hollow columns lead to strong angular variation of polarized reflectances that are not often seen in the POLDER data and it may hence be surprising that Sun et al. (2006) found these habits to fit most of the included data. The stringent data selection applied in this study as discussed in section 4.2.3 may have biased the data. On a regional spatial scale, Baran et al. (2015) investigated the local variation of crystals roughness inferred from multi-directional total reflectances in relation to relative humidity. Using a rather limited dataset off the coast of Great Britain, they concluded that the occurrence of pristine crystal mixtures are associated with relatively humid conditions. However, these interesting conclusions are based on only 12 POLDER pixels with inferred pristine particles and need to be confirmed using a larger dataset. In addition, biases from interference of lower liquid clouds could not be convincingly excluded.

From the list of dominating shapes in Table 1 and the discussion of remote sensing studies above, it is clear that the inferred shapes are highly dependent on which shapes are included in the investigation. For example, Cole et al. (2014) find aggregates of columns to be dominating globally but do not consider Koch fractals, while the opposite is true for Chepfer et al. (2001). Also, Cole et al. (2013) found a rough general mixture to fit most global data and severely roughened aggregates of columns to be a poor fit, while Cole et al. (2014) applied a wider range of roughness to all particles and came to the exact opposite conclusion, i.e., a dominance of aggregates of columns and hardly any data to be more consistent with the general mixture of habits with any roughness applied. Furthermore, Cole et al. (2013, 2014) found the inferred shapes and roughness values to be dependent on assumed crystal size. However, as also discussed in section 3, this size dependency largely stems from the fact that most of the assumed ice crystal model geometries (i.e., aspect ratios of the crystals or their components) depend on size. Thus, assuming a different size essentially changes the set of models considered in this case. As discussed in section 2, the geometry of the components of such complex crystals, and particularly their size dependency, is very poorly constrained. A general aspect of the studies discussed above is that they focus on the inference of either ice crystals habit, crystal roughness or a combination of the two. However, as discussed in section 3, the aspect ratio of the crystals or their components greatly affects the scattering properties and needs to be taken account in a systematic way when inferring ice crystals shapes from remote

sensing data. Without the systematic inclusion of aspect ratios and roughness values in the retrieval products the results from such remote sensing studies are difficult to interpret as demonstrated above.

A retrieval algorithm to infer the aspect ratios of crystals or their components in addition to particle roughness level from polarized reflectances is presented by van Diedenhoven et al. (2012a) and applied to measurements of RSP (van Diedenhoven et al., 2013) and POLDER-PARASOL (van Diedenhoven et al., 2014b). In essence, this approach uses hexagonal plates and columns as proxies for the components of more complex particles. Other than most other studies in Table 1, the method includes a large, nearly continuous range of aspect ratios and roughness values. A look up table of simulated polarized reflectances is used based on a database of optical properties for hexagonal plates and columns, which is calculated using the geometrics optics code developed by Macke et al. (1996b). The aspect ratio of columns is varied between 1 and 50 with 26 geometrically increasing steps. The aspect ratios of plates are the inverse of those for columns, for a total of 51 aspect ratios. The roughness parameter, as defined by Macke et al. (1996b), is varied between δ =0 and δ =0.7 in steps of 0.05. The aspect ratio and roughness parameter values that produce the simulated polarized reflectances that lead to the best fit to the measurements are considered the retrieved values. Furthermore, the asymmetry parameter is derived from the retrieved aspect ratio and roughness parameter per Fig. 3.

The retrieval technique was evaluated by van Diedenhoven et al. (2012a) using simulated measurements based on optical properties of smooth, moderately roughened and severely roughened solid plates, solid and hollow columns, solid and hollow bullet rosettes, droxtals, aggregates of columns and aggregates of plates, as well as several mixtures of these habits (Baum et al., 2005, 2011; Yang et al., 2015). The evaluation showed that particles with plate-like, column-like, smooth and rough components are generally correctly identified. For all particles the retrieved roughness parameters increase with increasing roughness of the particles assumed in the simulated measurements, as expected. As seen in Fig. 6, the ice crystal asymmetry parameters are generally retrieved to within 5%, or about 0.04 in absolute terms, largely independent of calibration errors, range and sampling density of scattering angles and random noise in the measurements. Since the asymmetry parameter is largely determined by the aspect ratio and roughness of the crystal components, this good agreement between retrieved and true asymmetry parameters suggests that aspect ratio and roughness parameters of the components of these complex particles are retrieved well by the method, although they were not explicitly evaluated by van Diedenhoven et al. (2012a). A detailed study on simulated clouds consisting of bullet rosettes with arms of varying aspect ratios and roughness values showed that the algorithm retrieves aspect ratios with a bias of 20% on average and the roughness parameter within 0.05 when cloud optical thickness is above 5 (van Diedenhoven et al., 2012a). Errors on retrieved aspect ratios increase with decreasing optical thickness. Interestingly, the method finds that the polarized reflectances of clouds consisting of hollow columns and hollow bullet rosettes most closely resemble those consisting of columns with high aspect ratio ($\alpha > 15$). This result makes sense since the walls of the hollow parts of the crystals are thin, resembling columns with high aspect ratios (see section 3 and Figs. 4 and 5). In addition, van Diedenhoven et al. (2012a) showed that asymmetry parameters of mixtures of smooth and rough complex particles as defined by (Baum et al., 2011) are also mostly retrieved within 5%. For mixtures of hexagonal columns and plates with varying aspect ratios and roughness values, van Diedenhoven et al. (2016a) showed that the average absolute errors between retrieved and the ensemble-average aspect ratio $\alpha_{\leq 1}$ are generally below 0.1. Furthermore, ensemble-average roughness parameters are

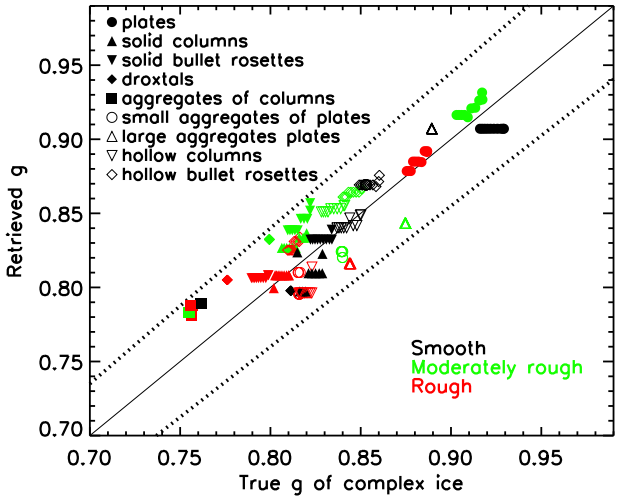

Figure 6. Asymmetry parameters retrieved with the method of van Diedenhoven et al. (2012a) from simulated data based on optical properties of several complex crystals plotted against the true asymmetry parameters of the complex crystals. Black, green and red colors are results for simulated data assuming smooth ($\sigma = 0$), moderately rough ($\sigma = 0.03$), and severely rough ($\sigma = 0.5$) particles, respectively. For each combination of roughness and habit, 10 different size distributions are applied. See van Diedenhoven et al. (2012a) for further details. The solid line shows the 1–1 line. Dotted lines indicate the targeted 5% accuracy limits. Figure reproduced from van Diedenhoven et al. (2012a).

generally retrieved within 0.1. Generally, the approach tends to be somewhat biased toward retrieving column-like crystals, although for about 75% of the test cases the dominating geometry was correctly determined. Furthermore, only considering mixtures that are dominated for over 3/4 by either plates or columns yielded the correct dominating geometry in about 90% of the cases.

van Diedenhoven et al. (2013) further evaluated this approach applied to measurements of the RSP instrument collected during the CRYSTAL-FACE campaign based in Florida in 2002. Four case studies were analyzed: two cases of thick convective clouds and two cases of thinner (detached) anvil cloud layers. In all cases the measurements indicate roughened ice crystals, consistent with previous findings. Retrieved aspect ratios in three cases were found to be close to unity, indicating that compact particles dominate the radiation, qualitatively consistent with CPI images where available. Retrievals for one contrasting anvil case indicate ice crystals consisting of plate-like components with aspect ratios around 0.3, consistent with the increased number of aggregates of plates seen in the CPI images obtained in this cloud layer.

An example of crystal properties varying per cloud type and conditions is illustrated in Fig. 7, which is derived from (previously unpublished) data of RSP and the Cloud Physics Lidar (CPL), both mounted on NASA's high-altitude ER-2 aircraft during the Studies of Emissions and Atmospheric Composition, Clouds and Climate Coupling by Regional Surveys (SEAC^{4}RS) campaign based out of Houston, Texas in 2013 (Toon et al., 2015). This figure also shows retrievals of ice effective radius (Eq.

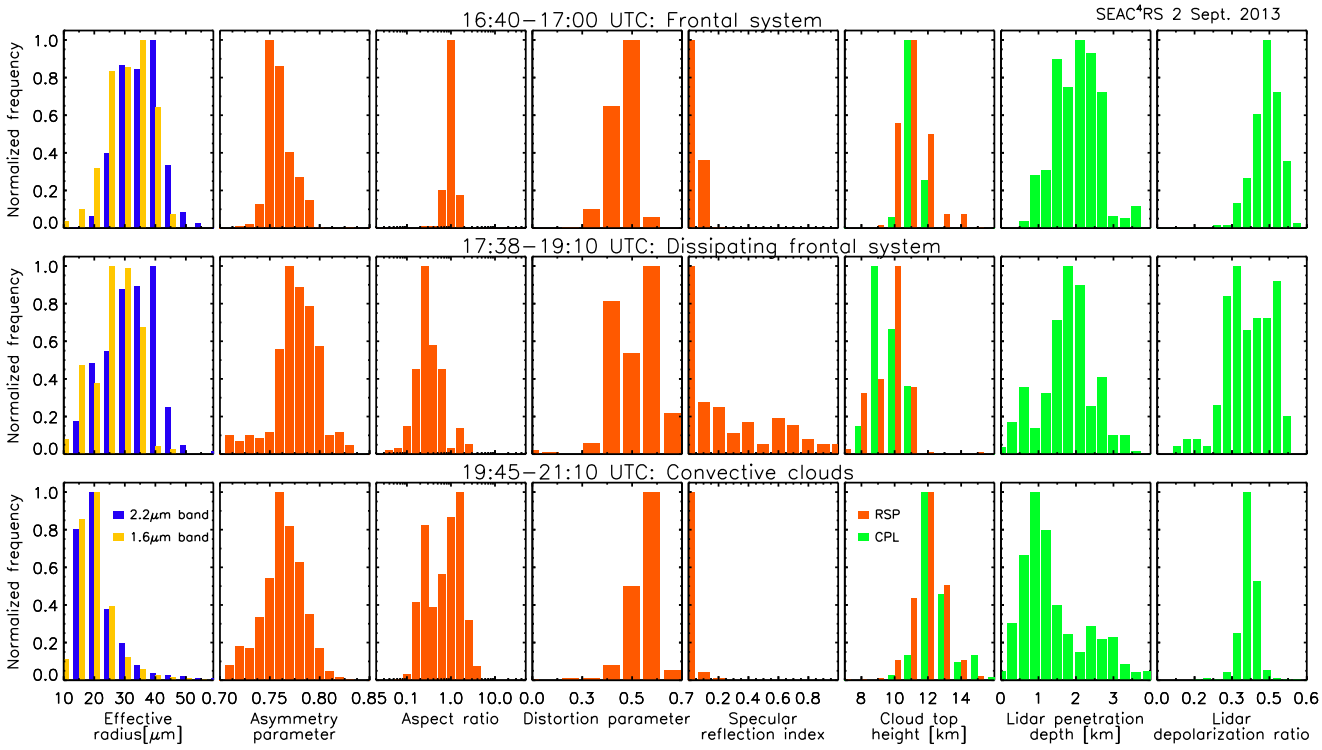

Figure 7. Histograms of ice cloud properties retrieved from measurements of RSP and CPL obtained on 2 September, 2013, during the SEAC^{4}RS campaign. From left to right respectively, the panels show the effective radii, asymmetry parameters, aspect ratios, roughness (or distortion) parameters δ, specular reflection index, cloud top heights, lidar penetration depths and depolarization ratios. Effective radii retrieved with the RSP channels at 1.59 and 2.26 μm are shown in yellow and blue, respectively. CPL retrieved quantities are shown in green. The top and middle panels show retrievals obtained during flight legs over a frontal cloud system in developing and dissipating stages, respectively. The bottom panel shows data for convective clouds over land. See text for more details.

12) using the shortwave infrared measurements on RSP (Nakajima and King, 1990; van Diedenhoven et al., 2014b, 2016b) as well as an index quantifying the strength of observed specular reflection in the RSP data (cf. Bréon and Dubrulle, 2004). For completeness, the cloud top height derived by RSP (Alexandrov et al., 2012; Sinclair et al., 2017) and CPL are also given, in addition to the CPL lidar depolarization and penetration depth. Here, CPL penetration depth indicates the physical depth at which CPL signals saturate, which is related to the mean extinction at cloud top (cf. van Diedenhoven et al., 2016b). Three different cloud conditions were observed on September 2nd, 2013. The top row of Fig. 7 shows retrievals for a frontal cloud system that was sampled, indicating a rather large variability in effective radius with a peak near 35–40 μm, cloud top heights at around 11 km and almost exclusively rough compact crystals with aspect ratios near unity, roughness parameters around 0.5 and asymmetry parameters near 0.75. The second row shows retrievals for the following hours, when the cloud system was

dissipating. Interestingly, the tops of these clouds seem to sublimate first, leaving the lower ice cloud layers visible to the RSP. The retrievals indicate plate-like particles with lower aspect ratios and a broader range of roughness values compared to the previous case. Observations of specular reflection indicates horizontally oriented ice plates were present in some regions. CPL depolarization ratios for these cloud layers are also lower compared to the earlier measurements, which might be caused by a change in ice habit, but may also be due to horizontally oriented crystals, especially in the case of depolarization values below 0.25. RSP effective radius values for these clouds range between 15 and 45 μm and considerable differences are seen between sizes retrieved with 2.26 and 1.59 μm bands, which implies substantial vertical variations of ice sizes (van Diedenhoven et al., 2016b). Finally, the third part of the day was devoted to sampling convection over land. The retrievals, shown in the third row, generally yield much smaller effective radii around 20 μm with almost no difference between retrievals using different spectral bands, indicating little vertical variation. This is consistent with relatively shallow lidar penetration depths for this case indicating compact and opaque cloud tops. The aspect ratios and asymmetry parameters show more variation than for the rest of the day, although lidar depolarization at cloud top has a narrower distribution. Furthermore, roughness parameters are somewhat larger for these convective clouds compared to the frontal system shown in the top row. This case study demonstrates the complex variability that can be observed in ice shapes and other properties of ice clouds. Furthermore, it shows the benefits of combining different retrievals techniques and instruments crucial to obtain a more complete view of ice cloud properties.

van Diedenhoven et al. (2014b) presented retrievals of ice crystals shape and asymmetry parameters from POLDER measurements collected off the north coast of Australia in relation with the Tropical Warm Pool - International Cloud Experiment (TWP-ICE) campaign in 2006 (May et al., 2008). The data are divided into periods of 4–9 days with alternating weak and strong convection, indicated by observed rain rates. Furthermore, the data is presented as a function of cloud top pressure and temperature, as ice crystal properties are generally observed to vary with temperature (e.g., Lawson et al., 2010; Noel et al., 2004, see also section 2). Only clouds with an optical thickness larger than 5 are included. The mean results shown in Fig. 8 indicate that mostly plate-like particle components with mean aspect ratios ($\alpha_{\leq 1}$) around 0.6 and low asymmetry parameters characterize strongly convective periods, while weakly convective periods generally show particles with larger asymmetry parameters, lower component aspect ratios, somewhat lower roughness parameters and more column-like crystal components. The abundance of compact plate-like crystals in the tops of convective clouds is consistent with previous observations of the dominance of compact and aggregated ice crystals with plate-like components observed in tropical deep convection (e.g., Noel et al., 2004; Connolly et al., 2005; Um and McFarquhar, 2009; Baran, 2009, see also section 2). There appears to be a trend towards lower aspect ratios and more column-like particles at warmer temperatures. The more column-like ice crystals with component aspect ratios further deviating from unity as indicated by the observations during the weakly convective periods may be consistent with a stronger contribution of particles grown in situ, which are more likely to form as crystals with column-like components, such as bullet rosettes, at the observed temperatures (Bailey and Hallett, 2009; Baran, 2009; Gallagher et al., 2012; Fridlind et al., 2016, see also Fig. 1). Comparing the results for the three strongly convective periods shows that microphysical parameters observed during the first two are very similar, while the third period shows somewhat greater roughness, fewer column-like crystals and lower asymmetry parameters. As shown by van Diedenhoven et al. (2014b), this later period also had substantially larger effective radii, especially at the warmer temperatures. The meteorological quantity

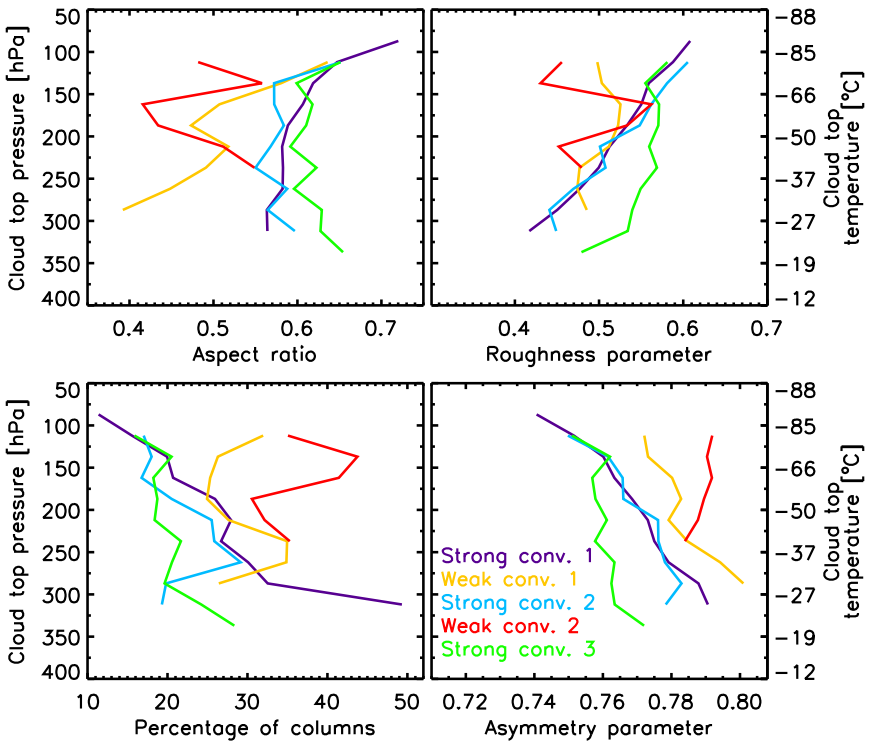

Figure 8. Mean ice crystal-component aspect ratio ($\alpha_{\leq 1}$, top left), roughness parameter (top right) and asymmetry parameter (bottom right) retrieved from POLDER-PARASOL data off the north coast of Australia between 16 January and 20 February, 2006. The percentage of retrieved column-like aspect ratios (i.e., $\alpha > 1$) is shown in the bottom left panel. Data within 25–hPa–wide cloud top pressure bins are averaged to produce profiles for five different periods (indicated by colors) with alternating strong and weak convective strengths. See text and van Diedenhoven et al. (2014b) for further details.

that possibly distinguishes the third strongly convective period from the other periods with strong convection is the middle-to-upper tropospheric zonal wind shear, which is much weaker for the third period and may have affected crystal evolution. For strongly convective periods, the roughness parameter values are about 0.55 on average and decrease significantly with increasing cloud top temperature, while asymmetry parameters increase. These results suggest systematic variations of crystals shape characteristics in relation to cloud top heights and atmospheric conditions. Such relationships need to be substantiated with more data. As demonstrated by van Diedenhoven et al. (2014b), such observed variations have significant impacts on the radiative properties of convective clouds, which need to be better understood to improve their representation in climate predictions.

In order to compare convective clouds observed in different atmospheric regimes, Fig. 9 shows histograms of ice crystal asymmetry parameters, aspect ratios and roughness parameters retrieved over convective clouds using 1) POLDER-PARASOL

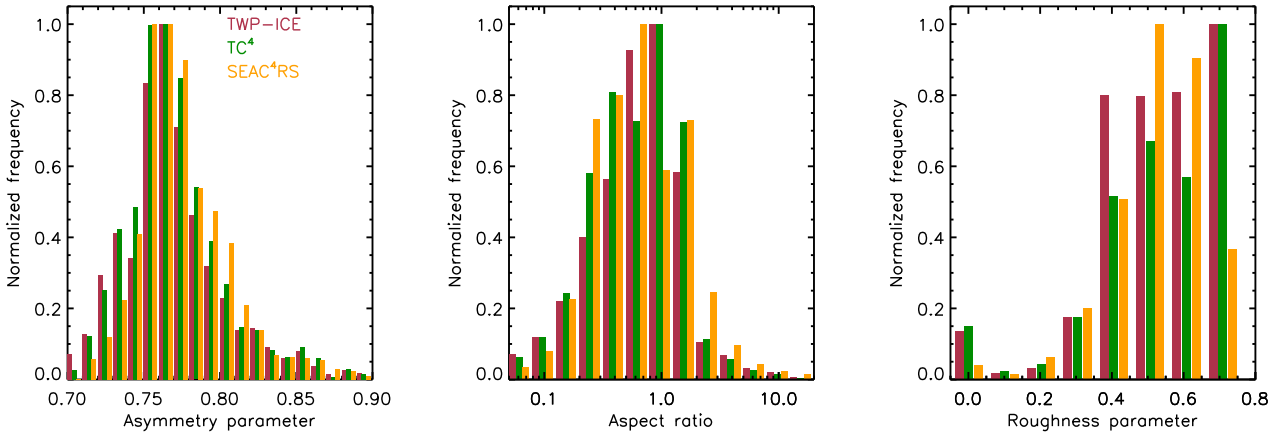

Figure 9. Histograms of the retrieved asymmetry parameters (left), aspect ratios (middle) and roughness parameters (right) for convective clouds observed in relation to the TWP-ICE (red), TC^4 (green) and $SEAC^4RS$ (yellow) campaigns.

data collected in relation with the TWP-ICE campaign (May et al., 2008; van Diedenhoven et al., 2014b); 2) POLDER-PARASOL data collected in relation to the TC^4 campaign (Toon et al., 2010) in 2007 near Costa Rica (previously unpublished); and 3) RSP data collected during the $SEAC^4RS$ campaign (Toon et al., 2015) based out of Houston, Texas in 2002 (cf. van Diedenhoven et al., 2016b). Only ice clouds with optical thicknesses larger than 5 are included in all data sets. Statistics of asymmetry parameters, aspect ratios and roughness parameters derived from these different datasets are very consistent. The data indicate crystals with mostly plate-like components ($\alpha < 1$), which is consistent with in situ measurements in convective clouds (e.g., Um and McFarquhar, 2009). Also, aspect ratios close to unity are mostly found, indicating the dominance of compact particles. Roughness values are generally large with maxima greater at 0.5, which is largely consistent with the roughness statistics found in tropical regions by Cole et al. (2014). Asymmetry parameters peak at around 0.76, but the distribution shows a substantial tail toward larger values.

In summary, results from retrieval approaches that focus on retrieving specific ice crystal habits are generally inconclusive and highly dependent on the shapes included in investigations. One general conclusion that can be derived from the various studies is that particle roughness is prevalent. However, roughness levels are found to vary with location, cloud top temperature, and atmospheric conditions. Systematic retrievals of crystal component aspect ratios show convective cloud regimes generally have crystals with aspect ratios close to unity and mostly plate-like particles, but the particle properties depend on multiple factors, e.g., cloud type, cloud height, convective strength and possibly other dynamical quantities as wind shear, as well as humidity. More global and local studies are needed to untangle such relationships between ice crystals shape and cloud type, cloud height and atmospheric conditions.

5 Prospective

Although many studies on remote sensing of ice crystals shapes using lidar and multi-directional reflectance data have been performed over the past few decades, the discussions in sections 4.1 and 4.2 show that it remains difficult to extract systematic conclusions from these studies. Specifically, robust quantitative interpretations of lidar depolarization measurements are still not available. As discussed in section 4.1, more research on optical properties calculations will likely improve the prospective of gaining quantitative information about ice crystals shapes from lidar measurements. Furthermore, measurements of a multi-static lidar, as proposed by Mishchenko et al. (2016), measuring the backscattered signal at additional angles and thus probing the depolarization properties at two or more angles could yield increased information content for the retrieval of ice crystal shape from lidars (cf. Smith et al., 2016). Combining colocated lidars at multiple wavelengths is not expected to increase potential for ice shape retrievals since the ice scattering properties are largely wavelength independent. Also high spectral resolution capability, such as included in ATLID and the airborne HSRL (Burton et al., 2015), is not expected to increase information content on ice crystal shapes, although it will provide valuable measurements of ice cloud extinction.

Currently, the POLDER instruments have been the only multi-directional polarimeters deployed in space. As polarimetry has great potential for cloud retrievals, as well as for the inference of aerosol properties, polarimeters are considered for many future satellite missions. For instance, the Multi-viewing, Multi-Channel Multi-Polarization Imaging instrument (3MI) is a follow-up version of POLDER and is planned to be included on the European MetOp series (Marbach et al., 2013). NASA's upcoming Plankton, Aerosol, Cloud, ocean Ecosystem (PACE) mission will likely include a multi-directional polarimeter. Furthermore, the Hyper-Angular Rainbow Polarimeter (HARP) instrument is a cubesat mission that is slated be be launched soon. Also the Multi-Angle Imager for Aerosols (MAIA) instrument is selected by NASA for further development and space deployment. It is expected that all these multi-directional polarimeters have potential for the retrieval of ice crystal shapes that is similar to or better than POLDER's. Interestingly, the 3MI instruments will in include a channel at around 1370 nm that is located on a strong water vapor absorption band. This limits the band's sensitivity to the surface and to liquid clouds in the lower atmosphere and increases the sensitivity to thin cirrus (cf. Gao et al., 1993). The RSP band at 1880 nm has similar capabilities and was used by Ottaviani et al. (2012) to infer the ice shape of a thin cirrus layer over the Deepwater Horizon oil spill site in 2010. Furthermore, the SPEX airborne polarimeter (Rietjens et al., 2015) yields multi-directional polarization measurements in the oxygen A-band that similarly shields the lower atmosphere and surface. Further statistical evaluation of such measurements will provide valuable statistics of thinner cirrus clouds, which are largely excluded from the current remote sensing results.

Ice crystal shape retrieval approaches have been largely limited to finding best fits to the measurements within look up tables of simulated measurements. It is advisable that more systematic inversion techniques are employed since these allow faster data processing, non-discrete solutions, and, more importantly, better error estimations (Rodgers, 2000). For example, Hioki et al. (2016) recently developed an algorithm based on empirical orthogonal function analysis of polarized reflectances to infer ice crystal roughness levels from such measurements. Approaches that retrieve quantifiable parameters such as ice crystal component aspect ratios and roughness parameters are especially suitable for the implementation in an algorithm employing

an inversion technique. The results of van Diedenhoven et al. (2016b) suggest that such an approach could infer the relative contribution of plate-like and columnar components to the ice crystal distributions, in addition to the mean aspect ratio ($\alpha_{\leq 1}$) and roughness parameter.

To date, few systematic investigations on the variation of crystal shape, aspect ratios and crystals roughness and their relation with cloud type, height and atmospheric conditions have been performed (e.g., Baran et al., 2016; Cole et al., 2014; van Diedenhoven et al., 2014b). More global and local studies are needed to untangle such relationships between ice crystals shape and cloud type, cloud height and atmospheric conditions. Such relationships will provide observational constraints for improved parameterizations of ice cloud optical properties (e.g., Baran et al., 2016) and for microphysical packages for cloud simulations, especially those explicitly prediction ice crystal shapes (e.g., Hashino et al., 2007, 2011; Harrington et al., 2013).

6 Conclusions

Improved constraints on the natural variation of ice crystal shapes is important since the shape of ice greatly affects their radiative and microphysical properties. Theoretical and laboratory studies show that ice crystal shapes largely depend on temperature and humidity of the environment in which they grew. However, in situ measurements in real ice clouds generally show complex mixtures of shapes and large contributions of irregular, complex, aggregated crystals. Also, the aspect ratios of components of these crystals are found to vary substantially. In addition, high magnification imaging of ice crystals show roughness structures of various forms and levels on the ice surfaces of growing and sublimating ice crystals. All of these macro- and microscale ice shape characteristics substantially affect the radiative properties of ice clouds and better constraints on how these shape characteristics vary with cloud type, temperature, humidity, locations, availability of aerosols, etcetera, are crucial to improve the representation of ice clouds in climate projections. This chapter reviews the current state of remote sensing of ice crystal macro- and microscale structure.

The radiative properties of clouds are determined by the number of ice crystals, their extinction cross sections, single scattering albedos and scattering phase matrices. Of these optical properties, the scattering phase matrix is especially relevant for the remote sensing of ice shapes, since it is substantially dependent to ice crystal shape but relatively independent to the size of ice crystals at non-absorbing wavelengths. The angular features in the scattering phase function and the linear polarization phase function that depend on ice crystals shape are used by remote sensing studies. Also the depolarization of backscattered polarized lidar signals is used to obtain information on ice crystal shape. Reviewing the dependencies of scattering phase matrices on ice shape reveals that the phase matrices are mostly determined by the aspect ratios of components of complex crystals as well as by the microscale structures such as crystal roughness, while the macroscale shape (i.e., habit) is of lesser importance. Furthermore, while ice particle macroscale shape has a seemingly endless variability and is not a quantifiable parameter, crystal component aspect ratio and roughness level are quantifiable and can be systematically related to variations in the phase matrix. For example, phase function asymmetry parameters increase as aspect ratios deviate from unity and decrease as roughness levels increase. It is therefore advised that remote sensing studies focus on retrieving information about crystal component aspect ratios and microscale structure, rather than on inferring the occurrence of specific ice habits.

A review of the literature on lidar depolarization measured in ice clouds shows that depolarization is generally found to increase with increasing cloud height and also varies with latitude. This variation is generally linked to the variation of ice crystal shape. However, the interpretation of the depolarization remains largely qualitative and inconclusive. For simple, smooth hexagonal prisms, lidar depolarization is shown to vary with crystal aspect ratio, but studies on the effects of crystal macroscale complexity, microscale roughness and hollowness are lacking, contradictory or inconclusive. More research on the relation between lidar depolarization and ice crystal shape is advised in order to move toward more quantitative inferences of ice crystal shape properties from lidar measurements.

Numerous studies evaluated the angular variation of total and/or polarized reflectances of ice clouds in order to infer information about ice crystal shape from them. A general conclusion is that ice crystal surface roughness or crystal distortion is prevalent. However, the conclusions about the dominating ice shapes are often contradictory. Furthermore, the data suggests that ice crystals shape and roughness is highly variable. Perusing the various studies, it is clear that the inferred shapes are strongly dependent on which shapes are included in the investigation and that such selections of shapes can be interpreted as rather arbitrary. Moreover, the specific geometries to define these shapes, most importantly the aspect ratios of their components, are very unconstrained. Since the inferred crystal shapes often do not agree with what is expected from in situ measurements and theory, the retrieved shapes are often interpreted as merely "radiative equivalent effective shapes" with no direct relation to ice crystal shapes in the observed clouds. However, focusing remote sensing applications on retrieving crystal component aspect ratio and particle roughness, rather than ice habit, yields useful physical information about these shape characteristics. Retrieval approaches that focus on inferring aspect ratios and/or roughness reveal that ice shapes depend on cloud height, latitude, cloud type, convective strength and possibly on humidity and dynamical quantities as wind shear. Statistics of ice crystal component aspect ratios, roughness parameters and asymmetry parameters of convective clouds in several different regimes are very comparable, suggesting generalized conclusions could be derived from such measurements. The data for these convective clouds indicate crystals with mostly compact plate-like components with high roughness levels are prevalent. Asymmetry parameters peak at around 0.76, but the distribution is substantially wide with a tail toward large values.

As is generally the case with all remote sensing products, the results in the current literature represents a subset of all ice clouds. Especially studies using multi-directional measurements are often biased to relatively optically thick ice clouds and thus excludes most cirrus. Improved data selection (e.g., Wang et al., 2014) and analysis of measurements obtained at wavelengths with substantial atmospheric gas absorption (e.g., Ottaviani et al., 2012) could yield more information about thin cirrus. Furthermore, the multi-directional total and polarized reflectances as well as lidar depolarization only yield information of the top 1–3 optical depths of clouds, while ice crystal shape is likely to vary vertically in clouds. This limitation also applies to retrievals of other cloud particle properties such as phase and size (Platnick, 2000; van Diedenhoven et al., 2016b). Hence, it is important to augment such retrievals with, e.g., in situ studies of the vertical variation of cloud particle properties. For convective clouds, however, statistics of cloud top trends of ice crystal properties can generally be used as surrogates for trends with height within convective cloud tops (referred to as time-space interchangeability, Lensky and Rosenfeld, 2006; van Diedenhoven et al., 2016b). Furthermore, cloud top properties are very relevant as the top of clouds can be considered as radiatively the most relevant part.

Lidar depolarization and multi-angular measurements, in addition to in situ observations, consistently reveal that ice crystal shape varies considerable with cloud top height, cloud type, location and atmospheric state. Ignoring these variations leads to biases in retrievals of ice effective radius and optical thickness that are sensitive to shape as well as to biases in simulations of ice cloud properties and their radiative effects. Research has begun to untangle such relationships between ice crystals shape and cloud type, cloud height and atmospheric conditions, but more studies are needed to reach systematic conclusions. Given the high potential of polarized lidar and multi-angle polarimeters for cloud and aerosol remote sensing, such instruments are planned or considered for many future satellite missions providing many future opportunities to further study the global variation of ice crystal shapes.

Acknowledgements. Bastiaan van Diedenhoven is supported by NASA under project numbers NNX14AJ28G and NNX15AD44G. I would like to thanks Dr. Nathan Magee at The College of New Jersey for providing the electron microscope images of hexagonal ice crystals images. I am grateful to Dr. Ping Yang for providing the optical properties of complex ice crystals.

References

Abdelmonem, A., Schnaiter, M., Amsler, P., Hesse, E., Meyer, J., and Leisner, T.: First correlated measurements of the shape and light scattering properties of cloud particles using the new Particle Habit Imaging and Polar Scattering (PHIPS) probe, Atm. Meas. Techn., 4, 2125–2142, doi:10.5194/amt-4-2125-2011, 2011.

Alexandrov, M. D., Cairns, B., Emde, C., Ackerman, A. S., and van Diedenhoven, B.: Accuracy assessments of cloud droplet size retrievals from polarized reflectance measurements by the Research Scanning Polarimeter, Remote Sens. Environ., 125, 92–111, doi:doi:10.1016/j.rse.2012.07.012, 2012.

Amsler, P., Stetzer, O., Schnaiter, M., Hesse, E., Benz, S., Moehler, O., and Lohmann, U.: Ice crystal habits from cloud chamber studies obtained by in-line holographic microscopy related to depolarization measurements, Appl. Opt., 48, 5811, doi:10.1364/AO.48.005811, 2009.

Auer, A. and Veal, D.: The dimension of ice crystals in natural clouds, J. Atmos. Sci, 27, 919–926, 1970.

aufm Kampe, H. J., Weickmann, H. K., Kelly, J. J., aufm Kampe, H. J., Weickmann, H. K., and Kelly, J. J.: The Influence of Temperature on the Shape of Ice Crystals Growing at Water Saturation, Journal of Meteorology, 8, 168–174, doi:10.1175/1520-0469(1951)008<0168:TIOTOT>2.0.CO;2, 1951.

Ávila, E. E., Castellano, N. E., Saunders, C. P. R., Bürgesser, R. E., and Aguirre Varela, G. G.: Initial stages of the riming process on ice crystals, Geophys. Res. Lett., 36, L09 808, doi:10.1029/2009GL037723, 2009.

Bailey, M., Hallett, J., Bailey, M., and Hallett, J.: Growth Rates and Habits of Ice Crystals between -20° and -70°C, J. Atmos. Sci., 61, 514–544, doi:10.1175/1520-0469(2004)061<0514:GRAHOI>2.0.CO;2, 2004.

Bailey, M., Hallett, J., Bailey, M., and Hallett, J.: Ice Crystal Linear Growth Rates from -20 to -70C: Confirmation from Wave Cloud Studies, J. Atmos. Sci., 69, 390–402, doi:10.1175/JAS-D-11-035.1, 2012.

Bailey, M. P. and Hallett, J.: A Comprehensive Habit Diagram for Atmospheric Ice Crystals: Confirmation from the Laboratory, AIRS II, and Other Field Studies, J. Atmos. Sci., 66, 2888–2899, doi:10.1175/2009JAS2883.1, 2009.

Baran, A. and C.-Labonnote, L.: On the reflection and polarisation properties of ice cloud, J. Quant. Spectrosc. Radiat. Transfer, 100, 41–54, 2006.

Baran, A. J.: A review of the light scattering properties of cirrus, J. Quant. Spectrosc. Radiat. Transfer, 110, 1239–1260, doi:10.1016/j.jqsrt.2009.02.026, 2009.

Baran, A. J. and C.-Labonnote, L.: A self-consistent scattering model for cirrus. I: The solar region, Q. J. R. Meteorol. Soc., 133, 1899–1912, doi:10.1002/qj.164, 2007.

Baran, A. J., Watts, P. D., and Foot, J. S.: Potential retrieval of dominating crystal habit and size using radiance data from a dual-view and multiwavelength instrument: A tropical cirrus anvil case, J. Geophys. Res., 103, 6075–6082, doi:10.1029/97JD03122, 1998.

Baran, A. J., Watts, P. D., and Francis, P. N.: Testing the coherence of cirrus microphysical and bulk properties retrieved from dual-viewing multispectral satellite radiance measurements, J. Geophys. Res., 104, 31 673–31 683, doi:10.1029/1999JD900842, 1999.

Baran, A. J., Furtado, K., Labonnote, L.-C., Havemann, S., Thelen, J.-C., and Marenco, F.: On the relationship between the scattering phase function of cirrus and the atmospheric state, Atm. Chem. Phys., 15, 1105–1127, doi:10.5194/acp-15-1105-2015, 2015.

Baran, A. J., Hill, P., Walters, D., Hardiman, S. C., Furtado, K., Field, P. R., Manners, J., Baran, A. J., Hill, P., Walters, D., Hardiman, S. C., Furtado, K., Field, P. R., and Manners, J.: The Impact of Two Coupled Cirrus Microphysics–Radiation Parameterizations

on the Temperature and Specific Humidity Biases in the Tropical Tropopause Layer in a Climate Model, J. Clim., 29, 5299–5316, doi:10.1175/JCLI-D-15-0821.1, 2016.

Baum, B. A., Yang, P., Heymsfield, A. J., Platnick, S., King, M. D., Hu, Y. X., and Bedka, S. M.: Bulk scattering properties for the remote sensing of ice clouds. Part II: Narrowband models, J. Appl. Meteor., 44, 1896–1911, 2005.

Baum, B. A., Yang, P., Hu, Y.-X., and Feng, Q.: The impact of ice particle roughness on the scattering phase matrix, J. Quant. Spectrosc. Radiat. Transfer, 111, 2534–2549, doi:10.1016/j.jqsrt.2010.07.008, 2010.

Baum, B. A., Yang, P., Heymsfield, A. J., Schmitt, C. G., Xie, Y., Bansemer, A., Hu, Y.-X., and Zhang, Z.: Improvements in shortwave bulk scattering and absorption models for the remote sensing of ice clouds, J. Appl. Meteor. Clim., 50, 1037–1056, doi:10.1175/2010JAMC2608.1, 2011.

Baum, B. A., Yang, P., Heymsfield, A. J., Bansemer, A., Cole, B. H., Merrelli, A., Schmitt, C., and Wang, C.: Ice cloud single-scattering property models with the full phase matrix at wavelengths from 0.2 to 100μm, J. Quant. Spectrosc. Radiat. Transfer, 146, 123–139, doi:10.1016/j.jqsrt.2014.02.029, 2014.

Bentley, W. A.: Some Recent Treasures of the Snow, Mon. Weather Rev., 55, 358–359, doi:10.1175/1520-0493(1927)55<358:SRTOTS>2.0.CO;2, 1927.

Berg, M. J., Sorensen, C. M., and Chakrabarti, A.: A new explanation of the extinction paradox, J. Quant. Spectrosc. Radiat. Transfer, 112, 1170–1181, doi:10.1016/j.jqsrt.2010.08.024, 2011.

Bi, L., Yang, P., Liu, C., Yi, B., Baum, B. A., van Diedenhoven, B., and Iwabuchi, H.: Assessment of the accuracy of the conventional ray-tracing technique: Implications in remote sensing and radiative transfer involving ice clouds, J. Quant. Spectrosc. Radiat. Transfer, 146, 158–174, doi:10.1016/j.jqsrt.2014.03.017, 2014.

Borovoi, A., Konoshonkin, A., and Kustova, N.: The physical-optics approximation and its application to light backscattering by hexagonal ice crystals, J. Quant. Spectrosc. Radiat. Transfer, 146, 181–189, doi:10.1016/j.jqsrt.2014.04.030, 2014.

Borovoi, A. G., Kustova, N. V., and Oppel, U. G.: Light backscattering by hexagonal ice crystal particles in the geometrical optics approximation, Opt. Eng., 44, 071 208, doi:10.1117/1.1955367, 2005.

Bourdages, L., Duck, T. J., Lesins, G., Drummond, J. R., and Eloranta, E. W.: Physical properties of high arctic tropospheric particles during winter, Atm. Chem. Phys., 9, 6881–6897, 2009.

Box, G. E. P.: Science and Statistics, J. Am. Stat. Assoc., 71, 791–799, doi:10.1080/01621459.1976.10480949, 1976.

Box, G. E. P. and Draper, N. R.: Empirical model-building and response surfaces, Wiley, 1987.

Bréon, F.-M. and Dubrulle, B.: Horizontally oriented plates in clouds, J. Atmos. Sci., 61, 2888–2898, doi:10.1175/JAS-3309.1, 2004.

Bryant, F. and Latimer, P.: Optical efficiencies of large particles of arbitrary shape and orientation, J. Colloid Interface Sci., 30, 291–304, doi:10.1016/0021-9797(69)90396-8, 1969.

Buriez, J.-C., Doutriaux-Boucher, M., Parol, F., Loeb, N. G., Buriez, J.-C., Doutriaux-Boucher, M., Parol, F., and Loeb, N. G.: Angular Variability of the Liquid Water Cloud Optical Thickness Retrieved from ADEOS–POLDER, J. Atmos. Sci., 58, 3007–3018, doi:10.1175/1520-0469(2001)058<3007:AVOTLW>2.0.CO;2, 2001.

Burton, S. P., Hair, J. W., Kahnert, M., Ferrare, R. A., Hostetler, C. A., Cook, A. L., Harper, D. B., Berkoff, T. A., Seaman, S. T., Collins, J. E., Fenn, M. A., and Rogers, R. R.: Observations of the spectral dependence of linear particle depolarization ratio of aerosols using NASA Langley airborne High Spectral Resolution Lidar, Atm. Chem. Phys., 15, 13 453–13 473, doi:10.5194/acp-15-13453-2015, 2015.

C.-Labonnote, L., Brogniez, G., Doutriaux-Boucher, M., Buriez, J., Gayet, J., and Chepfer, H.: Modeling of light scattering in cirrus clouds with inhomogeneous hexagonal monocrystals. Comparison with in-situ and ADEOS-POLDER measurements, Geophys. Res. Lett., 27, 113–116, doi:10.1029/1999GL010839, 2000.

C.-Labonnote, L., Brogniez, G., Buriez, J.-C., Doutriaux-Boucher, M., Gayet, J.-F., and Macke, A.: Polarized light scattering by inhomogeneous hexagonal monocrystals: Validation with ADEOS-POLDER measurements, J. Geophys. Res., 106, 12 139–12 153, doi:10.1029/2000JD900642, 2001.

Cairns, B., Russell, E. E., LaVeigne, J. D., and Tennant, P. M. W.: Research scanning polarimeter and airborne usage for remote sensing of aerosols, Proc. SPIE, 5158, 33–44, doi:10.1117/12.518320, 2003.

Chen, J. and Lamb, D.: The theoretical basis for the parameterization of ice crystal habits: Growth by vapor deposition, J. Atmos. Sci., 51, 1206–1222, doi:10.1175/1520-0469(1994)051<1206:TTBFTP>2.0.CO;2, 1994.

Chepfer, H., Brogniez, G., and Fouquart, Y.: Cirrus clouds' microphysical properties deduced from POLDER observations, J. Quant. Spectrosc. Radiat. Transfer, 60, 375–390, doi:10.1016/S0022-4073(98)00013-2, 1998.

Chepfer, H., Goloub, P., Riedi, J., De Haan, J., Hovenier, J., and Flamant, P.: Ice crystal shapes in cirrus clouds derived from POLDER/ADEOS-1, J. Geophys. Res, 106, 7955–7966, 2001.

Chepfer, H., Minnis, P., Young, D., Nguyen, L., and Arduini, R. F.: Estimation of cirrus cloud effective ice crystal shapes using visible reflectances from dual-satellite measurements, J. Geophys. Res., 107, AAC 21–1–AAC 21–16, doi:10.1029/2000JD000240, 2002.

Choi, Y.-S., Ho, C.-H., Kim, J., and Lindzen, R. S.: Satellite retrievals of (quasi-)spherical particles at cold temperatures, Geophys. Res. Lett., 37, 1–5, doi:10.1029/2009GL041818, 2010.

Coakley, J. A. J. and Chylek, P.: The two-stream approximation in radiative transfer: Including the angle of the incident radiation, J. Atmos. Sci., 32, 409–418, 1975.

Cole, B. H., Yang, P., Baum, B. A., Riedi, J., C.-Labonnote, L., Thieuleux, F., and Platnick, S.: Comparison of PARASOL observations with polarized reflectances simulated using different ice habit mixtures, J. Appl. Met. Climatol., 52, 186–196, doi:10.1175/JAMC-D-12-097.1, 2013.

Cole, B. H., Yang, P., Baum, B. A., Riedi, J., and C.-Labonnote, L.: Ice particle habit and surface roughness derived from PARASOL polarization measurements, Atm. Chem. Phys., 14, 3739–3750, doi:10.5194/acp-14-3739-2014, 2014.

Connolly, P. J., Saunders, C. P. R., Gallagher, M. W., Bower, K. N., Flynn, M. J., Choularton, T. W., Whiteway, J., and Lawson, R. P.: Aircraft observations of the influence of electric fields on the aggregation of ice crystals, Q. J. R. Meteorol. Soc., 131, 1695–1712, doi:10.1256/qj.03.217, 2005.

Cross, J. D.: Scanning Electron Microscopy of Evaporating Ice, Science, 164, 174–175, doi:10.1126/science.164.3876.174, 1969.

Del Guasta, M.: Simulation of LIDAR Returns from Pristine and Deformed Hexagonal Ice Prisms in Cold Cirrus by means of "Face Tracing", J. Geophys. Res., 106, 12 589–12 602, 2001.

Del Guasta, M., Vallar, E., Riviere, O., Castagnoli, F., Venturi, V., and Morandi, M.: Use of polarimetric lidar for the study of oriented ice plates in clouds, Appl. Opt., 45, 4878–4887, 2006.

Deschamps, P.-Y., Breon, F.-M., Leroy, M., Podaire, A., Bricaud, A., Buriez, J.-C., and Seze, G.: The POLDER mission: instrument characteristics and scientific objectives, IEEE Transactions on Geoscience and Remote Sensing, 32, 598–615, doi:10.1109/36.297978, 1994.

Diner, D., Beckert, J., Bothwell, G., and Rodriguez, J.: Performance of the MISR instrument during its first 20 months in Earth orbit, IEEE Trans. Geosci. Remote Sens., 40, 1449–1466, doi:10.1109/TGRS.2002.801584, 2002.

Diner, D. J., Xu, F., Garay, M. J., Martonchik, J. V., Rheingans, B. E., Geier, S., Davis, A., Hancock, B. R., Jovanovic, V. M., Bull, M. A., Capraro, K., Chipman, R. A., and McClain, S. C.: The Airborne Multiangle SpectroPolarimetric Imager (AirMSPI): a new tool for aerosol and cloud remote sensing, Atm. Meas. Techn., 6, 2007–2025, doi:10.5194/amt-6-2007-2013, 2013.

Doutriaux-Boucher, M., Buriez, J., Brogniez, G., C.-Labonnote, L., and Baran, A. J.: Sensitivity of retrieved POLDER directional cloud optical thickness to various ice particle models, Geophys. Res. Lett., 27, 109, doi:10.1029/1999GL010870, 2000.

Fougnie, B., Bracco, G., Lafrance, B., Ruffel, C., Hagolle, O., and Tinel, C.: PARASOL in-flight calibration and performance., Appl. Opt., 46, 5435–51, 2007.

Fridlind, A. M., Atlas, R., van Diedenhoven, B., Um, J., McFarquhar, G. M., Ackerman, A. S., Moyer, E. J., and Lawson, R. P.: Derivation of physical and optical properties of mid-latitude cirrus ice crystals for a size-resolved cloud microphysics model, Atm. Chem. Phys., 16, 7251–7283, doi:10.5194/acp-16-7251-2016, 2016.

Fu, Q.: A new parameterization of an asymmetry factor of cirrus clouds for climate models, J. Atmos. Sci., 64, 4140, doi:10.1175/2007JAS2289.1, 2007.

Furtado, K., Field, P. R., Cotton, R., and Baran, A. J.: The sensitivity of simulated high clouds to ice crystal fall speed, shape and size distribution, Q. J. R. Meteorol. Soc., 141, 1546–1559, doi:10.1002/qj.2457, 2015.

Gallagher, M. W., Connolly, P. J., Crawford, I., Heymsfield, A., Bower, K. N., Choularton, T. W., Allen, G., Flynn, M. J., Vaughan, G., and Hacker, J.: Observations and modelling of microphysical variability, aggregation and sedimentation in tropical anvil cirrus outflow regions, Atm. Chem. Phys., 12, 6609–6628, doi:10.5194/acp-12-6609-2012, 2012.

Gao, B., Goetz, A. F. H., and Wiscombe, W. J.: Cirrus cloud detection from Airborne Imaging Spectrometer data using the 1.38 μm water vapor band, Geophys. Res. Lett., 20, 301, doi:10.1029/93GL00106, 1993.

Geogdzhayev, I. and van Diedenhoven, B.: The effect of roughness model on scattering properties of ice crystals, J. Quant. Spectrosc. Radiat. Transfer, 178, 134–141, doi:10.1016/j.jqsrt.2016.03.001, 2016.

Gimmestad, G. G.: Reexamination of depolarization in lidar measurements, Appl. Opt., 47, 3795, doi:10.1364/AO.47.003795, 2008.

Gonda, T. and Yamazaki, T.: Morphology of ice droxtals grown from supercooled water droplets, J. Crystal Growth, 45, 66–69, doi:10.1016/0022-0248(78)90416-5, 1978.

Greenler, R.: Rainbows, halos, and glories, Cambridge University Press, 1990.

Gu, Y. and Liou, K. N.: Interactions of Radiation, Microphysics, and Turbulence in the Evolution of Cirrus Clouds., J. Atmos. Sci., 57, doi:http://dx.doi.org/10.1175/1520-0469(2000)057<2463:IORMAT>2.0.CO;2, 2000.

Gu, Y., Liou, K. N., Ou, S. C., and Fovell, R.: Cirrus cloud simulations using WRF with improved radiation parameterization and increased vertical resolution, J. Geophys. Res., 116, D06 119, doi:10.1029/2010JD014574, 2011.

Hallett, J. and Mason, B. J.: The Influence of Temperature and Supersaturation on the Habit of Ice Crystals Grown from the Vapour, Proc. Royal Soc. A, 247, 440–453, doi:10.1098/rspa.1958.0199, 1958.

Harrington, J. Y., Sulia, K., and Morrison, H.: A Method for Adaptive Habit Prediction in Bulk Microphysical Models. Part I: Theoretical Development., J. Atmos. Sci., 70, 349–363, doi:10.1175/JAS-D-12-040.1, 2013.

Hashino, T., Tripoli, G. J., Hashino, T., and Tripoli, G. J.: The Spectral Ice Habit Prediction System (SHIPS). Part I: Model Description and Simulation of the Vapor Deposition Process, J. Atmos. Sci., 64, 2210–2237, doi:10.1175/JAS3963.1, 2007.

Hashino, T., Tripoli, G. J., Hashino, T., and Tripoli, G. J.: The Spectral Ice Habit Prediction System (SHIPS). Part III: Description of the Ice Particle Model and the Habit-Dependent Aggregation Model, J. Atmos. Sci., 68, 1125–1141, doi:10.1175/2011JAS3666.1, 2011.

Heymsfield, A. and Andrew: Ice Crystal Terminal Velocities, J. Atmos. Sci., 29, 1348–1357, doi:10.1175/1520-0469(1972)029<1348:ICTV>2.0.CO;2, 1972.

Heymsfield, A. J., Lewis, S., Bansemer, A., Iaquinta, J., Miloshevich, L. M., Kajikawa, M., Twohy, C., Poellot, M. R., Heymsfield, A. J., Lewis, S., Bansemer, A., Iaquinta, J., Miloshevich, L. M., Kajikawa, M., Twohy, C., and Poellot, M. R.: A General Approach for Deriving the Properties of Cirrus and Stratiform Ice Cloud Particles, J. Atmos. Sci., 59, 3–29, doi:10.1175/1520-0469(2002)059<0003:AGAFDT>2.0.CO;2, 2002.

Hioki, S., Yang, P., Baum, B. A., Platnick, S., Meyer, K. G., King, M. D., and Riedi, J.: Degree of ice particle surface roughness inferred from polarimetric observations, Atm. Chem. Phys., 16, 7545–7558, doi:10.5194/acp-16-7545-2016, 2016.

Holz, R. E., Platnick, S., Meyer, K., Vaughan, M., Heidinger, A., Yang, P., Wind, G., Dutcher, S., Ackerman, S., Amarasinghe, N., Nagle, F., and Wang, C.: Resolving ice cloud optical thickness biases between CALIOP and MODIS using infrared retrievals, Atm. Chem. Phys., 16, 5075–5090, doi:10.5194/acp-16-5075-2016, 2016.

Hong, G. and Minnis, P.: Effects of spherical inclusions on scattering properties of small ice cloud particles, J. Geophys. Res., 120, 2951–2969, doi:10.1002/2014JD022494, 2015.

Hooke, R.: Micrographia, Warnock Library, London, 1665.

Hu, Y.-X., Winker, D., Yang, P., Baum, B., Poole, L., and Vann, L.: Identification of cloud phase from PICASSO-CENA lidar depolarization: a multiple scattering sensitivity study, J. Quant. Spectrosc. Radiat. Transfer, 70, 569–579, doi:10.1016/S0022-4073(01)00030-9, 2001.

Hudait, A. and Molinero, V.: What Determines the Ice Polymorph in Clouds?, J. Am. Chem. Soc., 138, 8958–8967, doi:10.1021/jacs.6b05227, 2016.

Iaquinta, J., Isaka, H., and Personne, P.: Scattering phase function of bullet rosette ice crystals, J. Atmos. Sci., 52, 1401–1413, doi:10.1175/1520-0469(1995)052<1401:SPFOBR>2.0.CO;2, 1995.

Jacobowitz, H.: A method for computing the transfer of solar radiation through clouds of hexagonal ice crystals, J. Quant. Spectrosc. Radiat. Transfer, 11, 691–695, doi:10.1016/0022-4073(71)90047-1, 1971.

Järvinen, E., Schnaiter, M., Mioche, G., Jourdan, O., Shcherbakov, V. N., Costa, A., Afchine, A., Krämer, M., Heidelberg, F., Jurkat, T., Voigt, C., Schlager, H., Nichman, L., Gallagher, M., Hirst, E., Schmitt, C., Bansemer, A., Heymsfield, A., Lawson, P., Tricoli, U., Pfeilsticker, K., Vochezer, P., Möhler, O., Leisner, T., Järvinen, E., Schnaiter, M., Mioche, G., Jourdan, O., Shcherbakov, V. N., Costa, A., Afchine, A., Krämer, M., Heidelberg, F., Jurkat, T., Voigt, C., Schlager, H., Nichman, L., Gallagher, M., Hirst, E., Schmitt, C., Bansemer, A., Heymsfield, A., Lawson, P., Tricoli, U., Pfeilsticker, K., Vochezer, P., Möhler, O., and Leisner, T.: Quasi-Spherical Ice in Convective Clouds, J. Atmos. Sci., 73, 3885–3910, doi:10.1175/JAS-D-15-0365.1, 2016.

Key, J. R., Yang, P., Baum, B. A., and Nasiri, S.: Parameterization of shortwave ice cloud optical properties for various particle habits, J. Geophys. Res., 107, 4181, doi:10.1029/2001JD000742, 2002.

Kikuchi, K., Kameda, T., Higuchi, K., and Yamashita, A.: A global classification of snow crystals, ice crystals, and solid precipitation based on observations from middle latitudes to polar regions, Atm. Res., 132, 460–472, doi:10.1016/j.atmosres.2013.06.006, 2013.

Knap, W. H., C.-Labonnote, L., Brogniez, G., and Stammes, P.: Modeling total and polarized reflectances of ice clouds: evaluation by means of POLDER and ATSR-2 measurements, Appl. Opt., 44, 4060, doi:10.1364/AO.44.004060, 2005.

Kokhanovsky, A.: The contrast and brightness of halos in crystalline clouds, Atm. Res., 89, 110–112, doi:10.1016/j.atmosres.2007.12.006, 2008.

Konoshonkin, A. V., Kustova, N. V., Shishko, V. A., and Borovoi, A. G.: The technique for solving the problem of light backscattering by ice crystals of cirrus clouds by the physical optics method for a lidar with zenith scanning, Atm. Oceanic Opt., 29, 252–262, doi:10.1134/S1024856016030088, 2016.

Korolev, A. V. and Isaac, G.: Roundness and aspect ratio of particles in ice clouds, J. Atmos. Sci., 60, 1795–1808, 2003.

Kuhs, W. F., Sippel, C., Falenty, A., and Hansen, T. C.: Extent and relevance of stacking disorder in "ice I(c)"., Proc. National Academy of Sciences, 109, 21 259–64, doi:10.1073/pnas.1210331110, 2012.

Lawson, R. P., Baker, B. A., Schmitt, C. G., and Jensen, T. L.: An overview of microphysical properties of Arctic clouds observed in May and July 1998 during FIRE ACE, J. Geophys. Res., 106, 14 989–15 014, doi:10.1029/2000JD900789, 2001.

Lawson, R. P., Baker, B., Pilson, B., and Mo, Q.: In situ observations of the microphysical properties of wave, cirrus, and anvil clouds. Part II: Cirrus clouds, J. Atmos. Sci., 63, 3186, doi:10.1175/JAS3803.1, 2006.

Lawson, R. P., Jensen, E., Mitchell, D. L., Baker, B., Mo, Q., and Pilson, B.: Microphysical and radiative properties of tropical clouds investigated in TC4 and NAMMA, J. Geophys. Res., 115, doi:10.1029/2009JD013017, 2010.

Lefebvre, A., Hélière, A., Pérez Albiñana, A., Wallace, K., Maeusli, D., Lemanczyk, J., Lusteau, C., Nakatsuka, H., and Tomita, E.: EarthCARE mission, overview, implementation approach and development status, in: Proc. SPIE, edited by Xiong, X. J., Kuriakose, S. A., and Kimura, T., vol. 9881, p. 98810P, doi:10.1117/12.2223955, 2016.

Lensky, I. M. and Rosenfeld, D.: The time-space exchangeability of satellite retrieved relations between cloud top temperature and particle effective radius, Atmospheric Chemistry and Physics, 6, 2887–2894, doi:10.5194/acp-6-2887-2006, 2006.

Letu, H., Ishimoto, H., Riedi, J., Nakajima, T. Y., C.-Labonnote, L., Baran, A. J., Nagao, T. M., and Sekiguchi, M.: Investigation of ice particle habits to be used for ice cloud remote sensing for the GCOM-C satellite mission, Atm. Chem. Phys., 16, 12 287–12 303, doi:10.5194/acp-16-12287-2016, 2016.

Lindqvist, H., Muinonen, K., Nousiainen, T., Um, J., McFarquhar, G. M., Haapanala, P., Makkonen, R., and Hakkarainen, H.: Ice-cloud particle habit classification using principal components, J. Geophys. Res., 117, doi:10.1029/2012JD017573, 2012.

Liou, K.-N. and Yang, P.: Light scattering by ice crystals : fundamentals and applications, Cambridge University Press, 2016.

Liu, C., Lee Panetta, R., and Yang, P.: The effects of surface roughness on the scattering properties of hexagonal columns with sizes from the Rayleigh to the geometric optics regimes, J. Quant. Spectrosc. Radiat. Transfer, 129, 169–185, doi:10.1016/j.jqsrt.2013.06.011, 2013.

Liu, C., Yang, P., Minnis, P., Loeb, N., Kato, S., Heymsfield, A., and Schmitt, C.: A two-habit model for the microphysical and optical properties of ice clouds, Atm. Chem. Phys., 14, 13 719–13 737, doi:10.5194/acp-14-13719-2014, 2014.

López, M. L. and Ávila, E. E.: Deformations of frozen droplets formed at -40°C, Geophys. Res. Lett., 39, doi:10.1029/2011GL050185, 2012.

Macke, A.: Scattering of Light by Polyhedral Ice Crystals, Appl. Opt., 32, 2780–2788, 1993.

Macke, A., Mishchenko, M. I., and Cairns, B.: The influence of inclusions on light scattering by large ice particles, J. Geophys. Res., 101, 23 311–23 316, doi:10.1029/96JD02364, 1996a.

Macke, A., Mueller, J., and Raschke, E.: Single scattering properties of atmospheric ice crystals, J. Atmos. Sci., 53, 2813–2825, 1996b.

Magee, N. B., Miller, A., Amaral, M., and Cumiskey, A.: Mesoscopic surface roughness of ice crystals pervasive across a wide range of ice crystal conditions, Atm. Chem. Phys., 14, 12 357–12 371, doi:10.5194/acp-14-12357-2014, 2014.

Magono, C. and Lee, C. W.: Meteorological classification of natural snow crystals, J. Fac. Sci., Hokkaido Univ., Ser. VII, 2, 321–355, 1966.

Malkin, T. L., Murray, B. J., Brukhno, A. V., Anwar, J., and Salzmann, C. G.: Structure of ice crystallized from supercooled water, Proc. National Academy of Sciences, 109, 1041–1045, doi:10.1073/pnas.1113059109, 2012.

Malkin, T. L., Murray, B. J., Salzmann, C. G., Molinero, V., Pickering, S. J., and Whale, T. F.: Stacking disorder in ice I, Phys. Chem. Chem. Phys., 17, 60–76, doi:10.1039/c4cp02893g, 2015.

Marbach, T., Phillips, P., Lacan, A., and Schlüssel, P.: The Multi-Viewing, -Channel, -Polarisation Imager (3MI) of the EUMETSAT Polar System - Second Generation (EPS-SG) dedicated to aerosol characterisation, in: Proc. SPIE, edited by Meynart, R., Neeck, S. P., and Shimoda, H., vol. 8889, p. 88890I, doi:10.1117/12.2028221, 2013.

Martins, E., Noel, V., and Chepfer, H.: Properties of cirrus and subvisible cirrus from nighttime Cloud-Aerosol Lidar with Orthogonal Polarization (CALIOP), related to atmospheric dynamics and water vapor, J. Geophys. Res, 116, D02 208, doi:10.1029/2010JD014519, 2011.

Mason, B. J.: The growth of ice crystals in a supercooled water cloud, Q. J. R. Meteorol. Soc., 79, 104–111, doi:10.1002/qj.49707933909, 1953.

Mason, B. J., Bryant, G. W., and Van den Heuvel, A. P.: The growth habits and surface structure of ice crystals, Philosophical Magazine, 8, 505–526, doi:10.1080/14786436308211150, 1963.

May, P. T., Mather, J. H., Vaughan, G., Jakob, C., McFarquhar, G. M., Bower, K. N., and Mace, G. G.: The Tropical Warm Pool International Cloud Experiment, Bull. Amer. Meteor. Soc., 89, 629, doi:10.1175/BAMS-89-5-629, 2008.

McFarlane, S. a. and Marchand, R. T.: Analysis of ice crystal habits derived from MISR and MODIS observations over the ARM Southern Great Plains site, J. Geophys. Res., 113, 1–17, doi:10.1029/2007JD009191, 2008.

Miao, J., Johnsen, K.-P., Buehler, S., and Kokhanovsky, A.: The potential of polarization measurements from space at mm and sub-mm wavelengths for determining cirrus cloud parameters, Atm. Chem. Phys., 3, 39–48, doi:10.5194/acp-3-39-2003, 2003.

Mie, G.: Beiträge zur Optik trüber Medien, speziell kolloidaler Metallösungen, Annalen der Physik, 330, 377–445, doi:10.1002/andp.19083300302, 1908.

Mishchenko, M. and Sassen, K.: Depolarization of lidar returns by small ice crystals: an application to contrails, Geophys. Res. Lett., 25, 101 029, 1998.

Mishchenko, M. I.: Light scattering by randomly oriented axially symmetric particles, J. Opt. Soc. America A, 8, 871, doi:10.1364/JOSAA.8.000871, 1991.

Mishchenko, M. I., Cairns, B., Kopp, G., Schueler, C. F., Fafaul, B. A., Hansen, J. E., Hooker, R. J., Itchkawich, T., Maring, H. B., and Travis, L. D.: Accurate Monitoring of Terrestrial Aerosols and Total Solar Irradiance: Introducing the Glory Mission, Bull. Am. Meteor. Soc., 88, 677, doi:10.1175/BAMS-88-5-677, 2007.

Mishchenko, M. I., Alexandrov, M. D., Cairns, B., and Travis, L. D.: Multistatic aerosol–cloud lidar in space: A theoretical perspective, J. Quant. Spectrosc. Radiat. Transfer, 184, 180–192, doi:10.1016/j.jqsrt.2016.07.015, 2016.

Mitchell, D. and Arnott, W.: A model predicting the evolution of ice particle size spectra and radiative properties of cirrus clouds. Part II: Dependence of absorption and extinction on ice crystal morphology, J. Atmos. Sci., 51, 817–832, doi:10.1175/1520-0469(1994)051<0817:AMPTEO>2.0.CO;2, 1994.

Mizuno, Y. and Yukiko: Studies of crystal imperfections in ice with reference to the growth process by the use of X-ray diffraction topography and divergent Laue method, J. Glaciology, 21, 409–418, 1978.

Murray, B. J., Salzmann, C. G., Heymsfield, A. J., Dobbie, S., III, R. R. N., Cox, C. J., Murray, B. J., Salzmann, C. G., Heymsfield, A. J., Dobbie, S., III, R. R. N., and Cox, C. J.: Trigonal Ice Crystals in Earth's Atmosphere, http://dx.doi.org/10.1175/BAMS-D-13-00128.1, 2015.

Nakajima, T. and King, M. D.: Determination of the optical thickness and effective particle radius of clouds from reflected solar radiation measurements. I - Theory, J. Atmos. Sci., 47, 1878–1893, doi:10.1175/1520-0469(1990)047<1878:DOTOTA>2.0.CO;2, 1990.

Nakaya, U.: Snow crystals - Natural and Artificial, Harvard Univ Press, 1954.

Neshyba, S. P., Lowen, B., Benning, M., Lawson, A., and Rowe, P. M.: Roughness metrics of prismatic facets of ice, J. Geophys. Res., 118, 3309–3318, doi:10.1002/jgrd.50357, 2013.

Noel, V., Chepfer, H., Ledanois, G., Delaval, A., and Flamant, P. H.: Classification of particle effective shape ratios in cirrus clouds based on the lidar depolarization ratio, Appl. Opt., 41, 4245, doi:10.1364/AO.41.004245, 2002.

Noel, V., Winker, D., McGill, M., and Lawson, P.: Classification of particle shapes from lidar depolarization ratios in convective ice clouds compared to in situ observations during CRYSTAL-FACE, J. Geophys. Res., 109, D24 213, doi:10.1029/2004JD004883, 2004.

Nousiainen, T., Lindqvist, H., McFarquhar, G. M., and Um, J.: Small irregular ice crystals in tropical cirrus, J. Atmos. Sci., 68, 2614–2627, doi:10.1175/2011JAS3733.1, 2011.

Nussenzveig, H. M.: The Theory of the Rainbow, Sci. Am., 236, 116–127, doi:10.1038/scientificamerican0477-116, 1977.

Ono, A.: The Shape and Riming Properties of Ice Crystals in Natural Clouds, doi:10.1175/1520-0469(1969)026<0138:TSARPO>2.0.CO;2, 1969.

Ottaviani, M., Cairns, B., Chowdhary, J., Van Diedenhoven, B., Knobelspiesse, K., Hostetler, C., Ferrare, R., Burton, S., Hair, J., Obland, M., and Rogers, R.: Polarimetric retrievals of surface and cirrus clouds properties in the region affected by the Deepwater Horizon oil spill, Remote Sens. Environ., 121, 389–403, doi:10.1016/j.rse.2012.02.016, 2012.

Panetta, R. L., Zhang, J.-N., Bi, L., Yang, P., and Tang, G.: Light scattering by hexagonal ice crystals with distributed inclusions, J. Quant. Spectrosc. Radiat. Transfer, 178, 336–349, doi:10.1016/j.jqsrt.2016.02.023, 2016.

Pauling, L.: The Structure and Entropy of Ice and of Other Crystals with Some Randomness of Atomic Arrangement, J. of the American Chemical Soc., 57, 2680–2684, doi:10.1021/ja01315a102, 1935.

Peltoniemi, J. I., Lumme, K., Muinonen, K., and Irvine, W. M.: Scattering of light by stochastically rough particles, Appl. Opt., 28, 4088, doi:10.1364/AO.28.004088, 1989.

Pfalzgraff, W. C., Hulscher, R. M., and Neshyba, S. P.: Scanning electron microscopy and molecular dynamics of surfaces of growing and ablating hexagonal ice crystals, Atm. Chem. Phys., 10, 2927–2935, doi:10.5194/acp-10-2927-2010, 2010.

Ping-Yü, H. and Needham, J.: Ancient Chinese Observations of Solar Haloes and Parhelia, Weather, 14, 124–134, doi:10.1002/j.1477-8696.1959.tb02450.x, 1959.

Platnick, S.: Vertical photon transport in cloud remote sensing problems, J. Geophys. Res., 105, 22 919–22 935, doi:10.1029/2000JD900333, 2000.

Reichardt, J., Reichardt, S., Hess, M., and McGee, T. J.: Correlations among the optical properties of cirrus-cloud particles: Microphysical interpretation, J. Geophys. Res., 107, AAC 8–1–AAC 8–12, doi:10.1029/2002JD002589, 2002.

Reichardt, J., Reichardt, S., Lin, R.-F., Hess, M., McGee, T. J., and Starr, D. O.: Optical-microphysical cirrus model, Journal of Geophysical Research, 113, D22 201, doi:10.1029/2008JD010071, 2008.

Riedi, J., Marchant, B., Platnick, S., Baum, B. A., Thieuleux, F., Oudard, C., Parol, F., Nicolas, J.-M., and Dubuisson, P.: Cloud thermodynamic phase inferred from merged POLDER and MODIS data, Atm. Chem. Phys., 10, 11 851–11 865, doi:10.5194/acp-10-11851-2010, 2010.

Rietjens, J. H. H., Smit, M., van Harten, G., Di Noia, A., Hasekamp, O. P., de Boer, J., Volten, H., Snik, F., and Keller, C. U.: Accurate spectrally modulating polarimeters for atmospheric aerosol characterization, in: Proc. SPIE, edited by Shaw, J. A. and LeMaster, D. A., vol. 9613, p. 96130S, doi:10.1117/12.2188024, 2015.

Rodgers, C.: Inverse methods for atmospheric sounding: Theory and practice, World Scientific, Singapore, 2000.

Rossow, W. B. and Schiffer, R. A.: Advances in understanding clouds from ISCCP., Bull. Amer. Meteor. Soc., 80, doi:10.1175/1520-0477(1999)080<2261:AIUCFI>2.0.CO;2, 1999.

Russotto, R. D., Ackerman, T. P., and Durran, D. R.: Sensitivity of thin cirrus clouds in the tropical tropopause layer to ice crystal shape and radiative absorption, J. Geophys. Res., 121, 2955–2972, doi:10.1002/2015JD024413, 2016.

Sassen, K.: Lidar Observations of High Plains Thunderstorm Precipitation, J. Atmos. Sci., 34, 1444–1457, doi:10.1175/1520-0469(1977)034<1444:LOOHPT>2.0.CO;2, 1977.

Sassen, K.: Rainbows in the Indian rock art of desert western America, Appl. Opt., 30, 3523, doi:10.1364/AO.30.003523, 1991.

Sassen, K.: Possible halo depictions in the prehistoric rock art of Utah, Appl. Opt., 33, 4756, doi:10.1364/AO.33.004756, 1994.

Sassen, K. and Benson, S.: A midlatitude cirrus cloud climatology from the facility for atmospheric remote sensing. Part II: Microphysical properties derived from lidar depolarization., J. Atmos. Sci., 58, 2103–2112, doi:10.1175/1520-0469(2001)058, 2001.

Sassen, K. and Petrilla, R. L.: Lidar depolarization from multiple scattering in marine stratus clouds, Appl. Opt., 25, 1450, doi:10.1364/AO.25.001450, 1986.

Sassen, K. and Zhu, J.: A global survey of CALIPSO linear depolarization ratios in ice clouds: Initial findings, J. Geophys. Res., 114, 1–12, doi:10.1029/2009JD012279, 2009.

Sassen, K., Zhu, J., and Benson, S.: Midlatitude cirrus cloud climatology from the facility for atmospheric remote sensing. IV. Optical displays, Appl. Opt., 42, 332, doi:10.1364/AO.42.000332, 2003.

Sassen, K., Kayetha, V. K., and Zhu, J.: Ice cloud depolarization for nadir and off-nadir CALIPSO measurements, Geophys. Res. Lett., 39, doi:10.1029/2012GL053116, 2012.

Sayer, A. M., Poulsen, C. A., Arnold, C., Campmany, E., Dean, S., Ewen, G. B. L., Grainger, R. G., Lawrence, B. N., Siddans, R., Thomas, G. E., and Watts, P. D.: Global retrieval of ATSR cloud parameters and evaluation (GRAPE): dataset assessment, Atm. Chem. Phys., 11, 3913–3936, doi:10.5194/acp-11-3913-2011, 2011.

Sazaki, G., Zepeda, S., Nakatsubo, S., Yokoyama, E., and Furukawa, Y.: Elementary steps at the surface of ice crystals visualized by advanced optical microscopy., PNAS, 107, 19 702–7, doi:10.1073/pnas.1008866107, 2010.

Schmidt, G. A., Kelley, M., Nazarenko, L., Ruedy, R., Russell, G. L., Aleinov, I., Bauer, M., Bauer, S. E., Bhat, M. K., Bleck, R., Canuto, V., Chen, Y.-H., Cheng, Y., Clune, T. L., Del Genio, A., de Fainchtein, R., Faluvegi, G., Hansen, J. E., Healy, R. J., Kiang, N. Y., Koch, D., Lacis, A. A., LeGrande, A. N., Lerner, J., Lo, K. K., Matthews, E. E., Menon, S., Miller, R. L., Oinas, V., Oloso, A. O., Perlwitz, J. P., Puma, M. J., Putman, W. M., Rind, D., Romanou, A., Sato, M., Shindell, D. T., Sun, S., Syed, R. A., Tausnev, N., Tsigaridis, K., Unger, N., Voulgarakis, A., Yao, M.-S., and Zhang, J.: Configuration and assessment of the GISS ModelE2 contributions to the CMIP5 archive, J. Adv. Modeling Earth Systems, 6, 141–184, doi:10.1002/2013MS000265, 2014.

Schmitt, C. G., Heymsfield, A. J., Schmitt, C. G., and Heymsfield, A. J.: On the Occurrence of Hollow Bullet Rosette– and Column-Shaped Ice Crystals in Midlatitude Cirrus, J. Atmos. Sci., 64, 4514–4519, doi:10.1175/2007JAS2317.1, 2007.

Schmitt, C. G., Schnaiter, M., Heymsfield, A. J., Yang, P., Hirst, E., Bansemer, A., Schmitt, C. G., Schnaiter, M., Heymsfield, A. J., Yang, P., Hirst, E., and Bansemer, A.: The microphysical properties of small ice particles measured by the Small Ice Detector - 3 probe during the MACPEX field campaign, J. Atmos. Sci., Early onli, JAS–D–16–0126.1, doi:10.1175/JAS-D-16-0126.1, 2016.

Schnaiter, M., Büttner, S., Möhler, O., Skrotzki, J., Vragel, M., and Wagner, R.: Influence of particle size and shape on the backscattering linear depolarisation ratio of small ice crystals – cloud chamber measurements in the context of contrail and cirrus microphysics, Atm. Chem. Phys., 12, 10 465–10 484, doi:10.5194/acp-12-10465-2012, 2012.

Schnaiter, M., Järvinen, E., Vochezer, P., Abdelmonem, A., Wagner, R., Jourdan, O., Mioche, G., Shcherbakov, V. N., Schmitt, C. G., Tricoli, U., Ulanowski, Z., and Heymsfield, A. J.: Cloud chamber experiments on the origin of ice crystal complexity in cirrus clouds, Atm. Chem. Phys., 16, 5091–5110, doi:10.5194/acp-16-5091-2016, 2016.

Schotland, R., Sassen, K., and Stone, R.: Observations by Lidar of linear depolarization ratios for hydrometeors, J. Appl. Met., 10, 1011–1017, 1971.

Shcherbakov, V., Gayet, J.-F., Jourdan, O., Ström, J., and Minikin, A.: Light scattering by single ice crystals of cirrus clouds, Geophys. Res. Lett., 33, L15 809, doi:10.1029/2006GL026055, 2006.

Sinclair, K., van Diedenhoven, B., Cairns, B., Yorks, J., Wasilewski, A., and McGill, M.: Remote Sensing of Multiple Cloud Layer Heights using Multi-Angular Measurements, Atm. Meas. Techn. Discuss., pp. 1–23, doi:10.5194/amt-2017-2, 2017.

Smith, H. R., Connolly, P. J., Baran, A. J., Hesse, E., Smedley, A. R., and Webb, A. R.: Cloud chamber laboratory investigations into scattering properties of hollow ice particles, J. Quant. Spectrosc. Radiat. Transfer, 157, 106–118, doi:10.1016/j.jqsrt.2015.02.015, 2015.

Smith, H. R., Connolly, P. J., Webb, A. R., and Baran, A. J.: Exact and near backscattering measurements of the linear depolarisation ratio of various ice crystal habits generated in a laboratory cloud chamber, J. Quant. Spectrosc. Radiat. Transfer, doi:10.1016/j.jqsrt.2016.01.030, 2016.

Stamnes, S., Ou, S., Lin, Z., Takano, Y., Tsay, S., Liou, K., and Stamnes, K.: Polarized radiative transfer of a cirrus cloud consisting of randomly oriented hexagonal ice crystals: The 3×3 approximation for non-spherical particles, J. Quant. Spectrosc. Radiat. Transfer, in press, doi:10.1016/j.jqsrt.2016.07.001, 2016.

Stephens, G. L., Tsay, S.-C., Stackhouse, Paul W., J., and Flatau, P. J.: The relevance of the microphysical and radiative properties of cirrus clouds to climate and climatic feedback, J. Atmos. Sci., 47, 1742–1754, 1990.

Stoelinga, M. T., Locatelli, J. D., Woods, C. P., Stoelinga, M. T., Locatelli, J. D., and Woods, C. P.: The Occurrence of "Irregular" Ice Particles in Stratiform Clouds, J. Atmos. Sci., 64, 2740–2750, doi:10.1175/JAS3962.1, 2007.

Sun, W., Loeb, N., and Yang, P.: On the retrieval of ice cloud particle shapes from POLDER measurements, J. Quant. Spectrosc. Radiat. Transfer, 101, 435–447, doi:10.1016/j.jqsrt.2006.02.071, 2006.

Sun, W., Baize, R. R., Videen, G., Hu, Y., and Fu, Q.: A method to retrieve super-thin cloud optical depth over ocean background with polarized sunlight, Atm. Chem. Phys., 15, 11 909–11 918, doi:10.5194/acp-15-11909-2015, 2015.

Takano, Y. and Liou, K.-N.: Solar Radiative Transfer in Cirrus Clouds. Part I: Single-Scattering and Optical Properties of Hexagonal Ice Crystals, J. Atmos. Sci., 46, 3–19, doi:10.1175/1520-0469(1989)046<0003:SRTICC>2.0.CO;2, 1989.

Tape, W.: Atmospheric halos, American Geophysical Union, 1994.

Tape, W. and Moilanen, J.: Atmospheric Halos and the Search for Angle X, vol. 58, American Geophysical Union, Washington, D. C., doi:10.1029/SP058, 2006.

Toon, O. B., Starr, D. O., Jensen, E. J., Newman, P. A., Platnick, S., Schoeberl, M. R., Wennberg, P. O., Wofsy, S. C., Kurylo, M. J., Maring, H., Jucks, K. W., Craig, M. S., Vasques, M. F., Pfister, L., Rosenlof, K. H., Selkirk, H. B., Colarco, P. R., Kawa, S. R., Mace, G. G., Minnis, P., and Pickering, K. E.: Planning, implementation, and first results of the Tropical Composition, Cloud and Climate Coupling Experiment (TC4), J. Geophys. Res., 115, D00J04, doi:10.1029/2009JD013073, 2010.

Toon, O. B., Maring, H., Dibb, J., Ferrare, R., Jacob, D. J., Jensen, E. J., Luo, Z. J., Mace, G. G., Pan, L. L., Pfister, L., Rosenlof, K. H., Redemann, J., Reid, J. S., Singh, H. B., Robert Yokelson, Minnis, P., Chen, G., Jucks, K. W., and Pszenny, A.: Planning, implementation and scientific goals of the Studies of Emissions and Atmospheric Composition, Clouds and Climate Coupling by Regional Surveys (SEAC4RS) field mission, J. Geophys. Res., Submitted, 2015.

Tyo, J. S., Goldstein, D. L., Chenault, D. B., and Shaw, J. A.: Review of passive imaging polarimetry for remote sensing applications., Appl. Opt., 45, 5453–69, 2006.

Ulanowski, Z., Kaye, P. H., Hirst, E., Greenaway, R. S., Cotton, R. J., Hesse, E., and Collier, C. T.: Incidence of rough and irregular atmospheric ice particles from Small Ice Detector 3 measurements, Atm. Chem. Phys., 14, 1649–1662, doi:10.5194/acp-14-1649-2014, 2014.

Um, J. and McFarquhar, G. M.: Single-Scattering Properties of Aggregates of Bullet Rosettes in Cirrus, J. Appl. Meteor. Climatol., 46, 757, doi:10.1175/JAM2501.1, 2007.

Um, J. and McFarquhar, G. M.: Single-scattering properties of aggregates of plates, Q. J. R. Meteorol. Soc, 135, 291–304, doi:10.1002/qj.378, 2009.

Um, J. and McFarquhar, G. M.: Formation of atmospheric halos and applicability of geometric optics for calculating single-scattering properties of hexagonal ice crystals: Impacts of aspect ratio and ice crystal size, J. Quant. Spectrosc. Radiat. Transfer, 165, 134–152, doi:10.1016/j.jqsrt.2015.07.001, 2015.

Um, J., McFarquhar, G. M., Hong, Y. P., Lee, S.-S., Jung, C. H., Lawson, R. P., and Mo, Q.: Dimensions and aspect ratios of natural ice crystals, Atm. Chem. Phys., 15, 3933–3956, doi:10.5194/acp-15-3933-2015, 2015.

van de Hulst, H. C.: Light scattering by small particles, Dover Publications, New York, 1957.

van Diedenhoven, B.: The prevalence of the 22° halo in cirrus clouds, J. Quant. Spectrosc. Radiat. Transfer, 146, 475–479, doi:10.1016/j.jqsrt.2014.01.012, 2014.

van Diedenhoven, B., Fridlind, A., Ackerman, A., Eloranta, E., and McFarquhar, G.: An evaluation of ice formation in large-eddy simulations of supercooled Arctic stratocumulus using ground-based lidar and cloud radar, J. Geophys. Res., 114, D10 203, doi:10.1029/2008JD011198, 2009.

van Diedenhoven, B., Fridlind, A., and Ackerman, A.: Influence of humidified aerosol on lidar depolarization measurements below ice-precipitating arctic stratus, J. Appl. Met. Climatol., 50, 2184–2192, doi:10.1175/JAMC-D-11-037.1, 2011.

van Diedenhoven, B., Cairns, B., Geogdzhayev, I. V., Fridlind, A. M., Ackerman, A. S., Yang, P., and Baum, B. A.: Remote sensing of ice crystal asymmetry parameter using multi-directional polarization measurements - Part 1: Methodology and evaluation with simulated measurements, Atm. Meas. Techn., 5, 2361–2374, doi:10.5194/amt-5-2361-2012, 2012a.

van Diedenhoven, B., Fridlind, A. M., Ackerman, A. S., and Cairns, B.: Evaluation of hydrometeor phase and ice properties in cloud-resolving model simulations of tropical deep convection using radiance and polarization measurements, J. Atmos. Sci., 69, 3290–3314, doi:10.1175/JAS-D-11-0314.1, 2012b.

van Diedenhoven, B., Cairns, B., Fridlind, A. M., Ackerman, A. S., and Garrett, T. J.: Remote sensing of ice crystal asymmetry parameter using multi-directional polarization measurements – Part 2: Application to the Research Scanning Polarimeter, Atm. Chem. Phys., 13, 3185–3203, doi:10.5194/acp-13-3185-2013, 2013.

van Diedenhoven, B., Ackerman, A., Cairns, B., and Fridlind, A.: A flexible parameterization for shortwave optical properties of ice crystals, J. Atmos. Sci., 71, 1763–1782, doi:10.1175/JAS-D-13-0205.1, 2014a.

van Diedenhoven, B., Fridlind, A. M., Cairns, B., and Ackerman, A. S.: Variation of ice crystal size, shape, and asymmetry parameter in tops of tropical deep convective clouds, J. Geophys. Res., 119, 11,809–11,825, doi:10.1002/2014JD022385, 2014b.

van Diedenhoven, B., Ackerman, A. S., Fridlind, A. M., Cairns, B., van Diedenhoven, B., Ackerman, A. S., Fridlind, A. M., and Cairns, B.: On Averaging Aspect Ratios and Distortion Parameters over Ice Crystal Population Ensembles for Estimating Effective Scattering Asymmetry Parameters, J. Atmos. Sci., 73, 775–787, doi:10.1175/JAS-D-15-0150.1, 2016a.

van Diedenhoven, B., Fridlind, A. M., Cairns, B., Ackerman, A. S., and Yorks, J. E.: Vertical variation of ice particle size in convective cloud tops, Geophys. Res. Lett., 43, 4586–4593, doi:10.1002/2016GL068548, 2016b.

Verschure, P.-P. H.: Thirty Years of Observing and Documenting Sky Optical Phenomena, Appl. Opt., 37, 1585, doi:10.1364/AO.37.001585, 1998.

Vouk, V.: Projected area of convex bodies., Nature, 162, 330, 1948.

Wang, C., Yang, P., Dessler, A., Baum, B. A., and Hu, Y.: Estimation of the cirrus cloud scattering phase function from satellite observations, J. Quant. Spectrosc. Radiat. Transfer, 138, 36–49, doi:10.1016/j.jqsrt.2014.02.001, 2014.

Weickmann, H. K.: Formen und Bildung atmosphärischer Eiskristalle, Beitr. Phys. fr. Atm., 28, 12–52, 1945.

Weitkamp, C., ed.: Lidar, range-resolved optical remote sensing of the atmosphere, Springer, New York, doi:10.1080/00107510902990209, 2005.

Wendling, P., Wendling, R., and Weickmann, H. K.: Scattering of solar radiation by hexagonal ice crystals, Appl. Opt., 18, 2663, doi:10.1364/AO.18.002663, 1979.

Winker, D. M., Hunt, W. H., and McGill, M. J.: Initial performance assessment of CALIOP, Geophys. Res. Lett., 34, L19 803, doi:10.1029/2007GL030135, 2007.

Wyser, K. and Yang, P.: Average ice crystal size and bulk short-wave single-scattering properties of cirrus clouds, Atmos. Res., 49, 315–335, doi:10.1016/S0169-8095(98)00083-0, 1998.

Xie, Y., Yang, P., Kattawar, G. W., Baum, B. A., and Hu, Y.: Simulation of the optical properties of plate aggregates for application to the remote sensing of cirrus clouds, Appl. Opt., 50, 1065, doi:10.1364/AO.50.001065, 2011.

Yang, P. and Fu, Q.: Dependence of ice crystal optical properties on particle aspect ratio, J. Quant. Spectrosc. Radiat. Transfer, 110, 1604–1614, doi:10.1016/j.jqsrt.2009.03.004, 2009.

Yang, P. and Liou, K.: Single-scattering Properties of Complex Ice Crystals in Terrestrial Atmosphere, Contr. Atmos. Phys., 71, 223–248, 1998.

Yang, P., Hong, G., Kattawar, G., and Minnis, P.: Uncertainties associated with the surface texture of ice particles in satellite-based retrieval of cirrus clouds: Part II - Effect of particle surface roughness on retrieved cloud optical thickness and effective particle size, IEEE Trans. Geosci. Rem. Sens., 46, 1948–1957, doi:10.1109/TGRS.2008.916472, 2008a.

Yang, P., Zhang, Z., Kattawar, G. W., Warren, S. G., Baum, B. A., Huang, H.-L., Hu, Y. X., Winker, D., and Iaquinta, J.: Effect of cavities on the optical properties of bullet rosettes: Implications for active and passive remote sensing of ice cloud properties, J. Appl. Meteor. Clim., 47, 2311–2330, doi:10.1175/2008JAMC1905.1, 2008b.

Yang, P., Bi, L., Baum, B. A., Liou, K.-N., Kattawar, G. W., Mishchenko, M. I., and Cole, B.: Spectrally Consistent Scattering, Absorption, and Polarization Properties of Atmospheric Ice Crystals at Wavelengths from 0.2 to 100 μ m, J. Atmos. Sci., 70, 330–347, doi:10.1175/JAS-D-12-039.1, 2013.

Yang, P., Liou, K.-N., Bi, L., Liu, C., Yi, B., and Baum, B. A.: On the radiative properties of ice clouds: Light scattering, remote sensing, and radiation parameterization, Adv. Atm. Sci., 32, 32–63, doi:10.1007/s00376-014-0011-z, 2015.

Yi, B., Yang, P., Baum, B. A., L'Ecuyer, T., Oreopoulos, L., Mlawer, E. J., Heymsfield, A. J., and Liou, K.-N.: Influence of Ice Particle Surface Roughening on the Global Cloud Radiative Effect, J. Atmos. Sci., 70, 2794–2807, doi:10.1175/JAS-D-13-020.1, 2013.

Yorks, J. E., Hlavka, D. L., Hart, W. D., and McGill, M. J.: Statistics of Cloud Optical Properties from Airborne Lidar Measurements, J. Atmos. Oceanic Technol., 28, 869–883, 2011.

Zakharova, N. T. and Mishchenko, M. I.: Scattering properties of needlelike and platelike ice spheroids with moderate size parameters, Appl. Opt., 39, 5052, doi:10.1364/AO.39.005052, 2000.

Zhang, Z., Yang, P., Kattawar, G., Riedi, J., Baum, B. A., Platnick, S., and Huang, H.: Influence of ice particle model on satellite ice cloud retrieval: Lessons learned from MODIS and POLDER cloud product comparison, Atm. Chem. Phys., 9, 7115–7129, 2009.

Zhou, C., Yang, P., Dessler, A. E., Hu, Y., and Baum, B. A.: Study of horizontally oriented ice crystals with CALIPSO observations and comparison with Monte Carlo radiative transfer simulations, J. Appl. Meteor. Climatol., 59, 1426–1439, doi:10.1175/JAMC-D-11-0265.1, 2012.